Archaeological and Anthropological Sciences (2022) 14:215
https://doi.org/10.1007/s12520-022-01680-6

ORIGINAL PAPER

Middle Pleistocene hominin teeth from Biache-Saint-Vaast, France

Laura Martín-Francés[1,2,3,4,5] · José María Bermúdez de Castro[3,6] · Marina Martínez de Pinillos[3] · María Martinón-Torres[3,6] · Juan Luis Arsuaga[1,2] · Benoît Bertrand[7] · Amélie Vialet[8]

Received: 29 April 2022 / Accepted: 4 October 2022 / Published online: 20 October 2022

Abstract

The study of dental morphology can be a very useful tool to understand the origin and evolution of Neanderthals in Europe during the Middle Pleistocene (MP). At present, the earliest evidence, ca. 430 ka, of a pre-Neanderthal population in Europe is the hominin sample from Atapuerca-Sima de los Huesos (SH) that present clear dental affinities with Neanderthals while other penecontemporaneous populations, such as Arago or Mala Balanica, exhibit less Neanderthal traits. We present the morphometric study of the external and internal dental structures of eleven hominin dental remains recovered from the MP, ca. 240 ka, French site of Biache-Saint-Vaast (BSV). Our analyses place the BSV hominins within the MP group, together with SH, Fontana Ranuccio, Visogliano, Steinheim or Montmaurin, that show greater morphological affinities with Neanderthals. Moreover, we identified interpopulation variability in the expression of the enamel thickness trait, with BSV hominins sharing the unique combination of thin and thick pattern in the premolars and molars with the SH population. These results further support the coexistence of two or more populations in Europe during the MP that reflect the population and settlement of human groups suggested by the Central Area of Dispersals of Eurasia (CADE) and sink and source model.

Keywords Dental morphometrics · µCT · Middle Pleistocene hominins · Neanderthals · Europe

Introduction

Providing new evidence on the diversity of the European Middle Pleistocene (MP) populations is relevant for the discussion on the origin of the Neanderthal clade. The great morphological variability in the combination of dental and cranial features in the European MP fossil record suggests a non-linear evolutionary scenario characterised by genetic drift, founder effect, isolation and hybridization of the populations (e.g. Bermúdez de Castro et al. 2019; Daura et al. 2017; Martínez de Pinillos et al. 2020; Roksandic et al. 2011). Within this framework, the sink and source model with a central area of dispersal in Eurasia (Bermúdez de Castro and Martinón-Torres 2013; Dennell et al. 2011) has been proposed as a more parsimonious explanation for the non-linear evolution of the MP groups towards the classic Neanderthals. In this model, the geographical and climatic constrains of Europe constituted a driving force in the demographic dynamics (Dennell et al. 2011). Amongst European MP fossils, the Atapuerca-Sima de los Huesos (Spain), Steinheim (Germany), Montmaurin (France), Swanscombe and Pontnewydd (UK) and Fontana Ranuccio and Visogliano (Italy) exhibit in their dentitions

✉ Laura Martín-Francés
lauramartinfrancesmf@gmail.com

1 Centro Mixto Universidad Complutense de Madrid - Instituto de Salud Carlos III de Evolución y Comportamiento Humanos, 28029 Madrid, Spain

2 Departamento de Paleontología, Facultad de Ciencias Geológicas, Universidad Complutense de Madrid, 28040 Madrid, Spain

3 CENIEH (National Research Center on Human Evolution), Paseo de la Sierra de Atapuerca 3, 09002 Burgos, Spain

4 Institut Català de Paleoecologia Humana i Evolució Social (IPHES), Zona Educacional 4, Campus Sescelades URV (Edifici W3), 43700 Tarragona, Spain

5 Departament d'Història i Història de l'Art, Universitat Rovira i Virgili, Avinguda de Catalunya 35, 43002 Tarragona, Spain

6 University College London Anthropology, London, UK

7 Univ. Lille, CHU Lille, ULR 7367 - UTML&A - Unité de Taphonomie Médico-Légale & d'Anatomie, 59000 Lille, France

8 Muséum National d'Histoire Naturelle, UMR7194, UPVD, 75013 Paris, France

a suite of features characteristic of the Neanderthal clade (Bermúdez de Castro et al. 2019; Martínez de Pinillos et al. 2017, 2020; Martinón-Torres et al. 2012; Vialet et al. 2018; Zanolli et al. 2018). In other European MP specimens, such as those of Ceprano (Italy), Aroeira (Portugal), Mala Balanica (Serbia) and Arago (France), the Neanderthal affinities are less clear (e.g. Bermúdez de Castro et al. 2019; Daura et al. 2017; Manzi, 2016; Roksandic 2016; Roksandic et al. 2011; Skinner et al. 2016) attesting for the possible coexistence of at least two hominin lineages in the European MP (e.g. Bermúdez de Castro et al. 2016; Dennell et al. 2011; MacDonald et al. 2012).

This work presents the outer and inner description and comparison of the MP remains from Biache-Saint-Vaast (BSV) with the aim of actively contributing to the understanding of the European MP evolutionary scenario. In particular, its comparison with other MP key sites showing different degrees of affinities with Neanderthals, amongst others Atapuerca-Sima de los Huesos (SH), dated 430 ka (Arsuaga et al. 2014; Demuro et al. 2019), and Arago, dated 450–400 ka (Falguères et al. 2015; Yokoyama et al. 1985; Yokoyama and Nguyen 1981), will help us to explore the hypothesis of different lineages in the European MP.

The BSV site is located 17 km east of the city of Arras (Pas-de-Calais Department), in northern France, at an altitude of about 50 m above sea level. It is an open-air site, located in the river deposits of the left bank of the Scarpe River. The site was discovered in 1976 while earthworks were being carried out for the construction of a metallurgical factory. Alain Tuffreau led an emergency excavation between 1976 and 1982 to save the site (Tuffreau 1978; Tuffreau et al. 1982). Sommé (1988) studied the stratigraphic sequence and observed several archaeological levels in the sequence of the lower terrace, most dating from the same period. In 1976, the first hominin skull was found in grid 9M (Tuffreau et al. 1982), at the base of level IIa of the complex 2b (BSV1), whereas cranial fragments of a second specimen were found in 1986 when P. Auguste was reviewing the fauna remains recovered from level IIa. Those remains (BSV2) came from grid 22T and belong to a second individual (Tuffreau, 1988). The hominin remains were associated to a rich lithic and faunal context. First dating analyses, including OSL and ESR, provided ages of 175±13 ka (Huxtable and Aikten 1988) and 253 + 53/– 37 ka (Yokoyama 1989), respectively. Moreover, fauna remains and pollen analyses (Sommé 1988) indicate a deposit episode for the human remains during the MIS 7 (between 240 and 190 ka; Lisiecki and Raymo 2005). A recent ESR/U-series analysis of several faunal remains associated to the paleoanthropological and archaeological remains provided a mean age of ca. 240 ka (Bahain et al. 2015), correlating the human occupation to MIS 7c. However, an older chronology can reasonably not be excluded for the site given the dating result of 332 ± 28 ka obtained for the only tooth of the study that do not show uranium leaching (Bahain et al. 2015).

Although Rougier (2003) performed the first description of the dental remains recovered from BSV, we aim to present a more detailed morphometric assessment of the dental remains by providing new insights on the external (OES) and internal (EDJ) morphological features as well as dental tissue proportions. With these analyses, we expect to explore the degree of affinity of BSV with other European MP hominins and Neanderthals and, ultimately, to shed light on the evolution of the Neanderthal clade.

Materials and methods

The dental sample under study comprises eleven maxillary teeth (Fig. 1; Table 1) including four isolated specimens (a left I^2, right and left P^3s, and right and left P^4s) and the right and left molar series (M^1–M^3) included in two maxillary fragments. The comparative sample comprises 224 teeth (including original data and from the literature) belonging to European MP hominins, Neanderthals, fossil *H. sapiens* and modern humans (Table 1). Due to limited mCT data access, we could not include the same sample for all the analyses (e.g. Arago). In addition, since some of the analyses are wear-dependent the number of specimens may vary for each analysis (Table 1 describes the sample included in each analysis).

Scanning of the samples

For this study, high-resolution µCT scanning of the fossil and modern material was performed in two laboratories. The BSV teeth were scanned at the Muséum National d'Histoire Naturelle, France (AST-RX Platform), and the modern human collections at CENIEH, Spain. The BSV maxillary remains and isolated teeth were scanned using a GE 103 Phoenix v/tome/x_L 450 instrument. The scanning of the isolated remains (I^2, P^3s and P^4) was performed using the following parameters: 120 kV and 180 µA, 0.5 mm Cu filter and isometric voxel size of 22 µm, while the scanning of the right and left maxillary fragments including M^1, M^2 and M^3 was performed at 100 kV and 410 µA, 0.4 mm Cu filter and resulting isometric voxel size of 41 µm. Finally, the modern human sample was scanned with a GE 103 Phoenix v/tome/x_s 240 instrument (CENIEH) with the following parameters: 100 kV and 100 µA, 0.2 mm Cu filter and isometric voxel size of 18µm.

Virtual segmentation

3D virtual segmentation of the dental tissues (enamel, dentine and pulp) was performed in Amira (6.3.0, FEI Inc.)

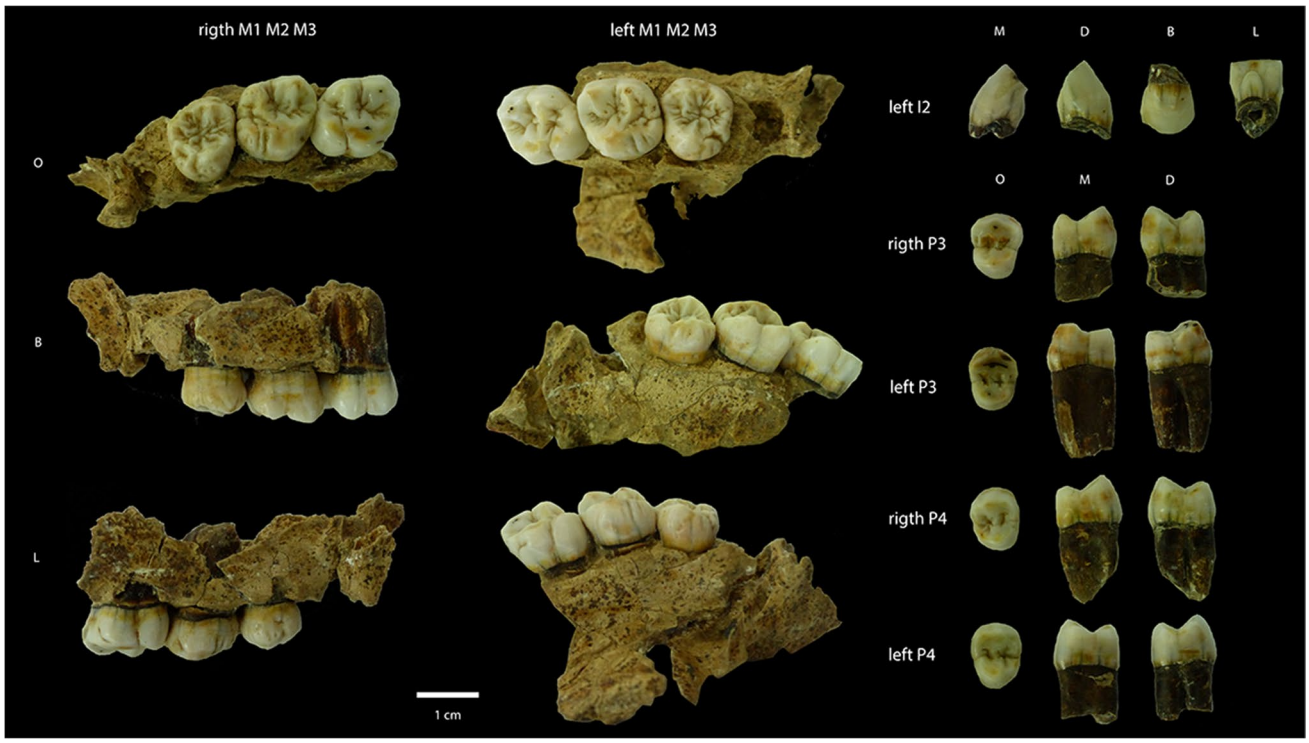

Fig. 1 Biache-Saint-Vaast (BSV) maxillary dental remains

using the semiautomatic tool, threshold-based segmentation, for the characterisation of the enamel-dentine junction (EDJ) morphology, tissue proportions and enamel thickness topographic distribution.

Metrics

Metric analyses comprised several approaches, including (a) mesio-distal (MD) and bucco-lingual (BL) diameter, crown index (CI) and total computed crown base area (TCBA) of the BSV dental sample (Table 2), and (b) relative occlusal polygon area (ROPA) and cusp angles of the BVS right M^1 (Tables 3 and 4). For the MD and BL diameters as well as for CI and TCBA (Tables 5, 6, 7 and 8), we compared the BSV results to those of SH, Arago, Neanderthals and Krapina samples (Bermúdez de Castro 1993; Bermúdez de Castro et al. 1999, 2019; Wolpoff 1979). Finally, for the ROPA variable and cusp angles, we compared the BSV estimates to those published for *H. antecessor*, SH, *H. heidelbergensis*, Neanderthals and *H. sapiens* (Bailey 2004; Martinón-Torres et al. 2013).

Morphological characterisation of the OES and EDJ

For the characterisation of the BSV enamel (OES) morphological traits and its comparison with other hominin samples, we employed the modified version of the Arizona State University Dental Anthropological System (Turner et al. 1991) by Martinón-Torres et al. (2012 and references therein).

Since there is not a scoring system for the non-metric traits at the dentine level, we employed the modified ASU-DAS system for OES (Martinón-Torres et al. 2012) to assess the morphological traits of the BSV and comparative sample (Table 9; SI Tables S1–S3). Moreover, for the Carabelli's trait, we followed the score system by Ortiz et al. (2012). Comparative sample includes the original dental remains of SH, Neanderthals and modern humans, as well as published data on Visogliano, Neanderthals and fossil *H. sapiens* (Zanolli et al. 2018, 2019).

Tissue proportions

For 3D tissue proportions assessment (Kono 2004; Olejniczak et al. 2008), we measured volume of enamel (Ve in mm^3); volume of coronal dentine including the pulp enclosed in the crown (Vcdp in mm^3); total volume of the crown, including the enamel, dentine and pulp (Vc in mm^3); and surface of the EDJ (SEDJ in mm^2) and calculated the 3D average enamel thickness (3D AET=Ve/SEDJ in mm); 3D relative enamel thickness (3D RET=100*3D AET/($Vcdp^{1/3}$), a scale-free measurement); and percentage of dentine and pulp in the total crown volume (Vcdp/Vc = 100*Vcdp/Vc in %). Comparative sample includes original data: TD6, SH

Table 1 Sample included in this study used for morphometric analyses

Site	Sample	Locality	Chronology	MIS	N	EDJ morphology (*N* total)	GM of the EDJ (*N* total)	Enamel thickness (*N* total)	Reference
Biache-Saint-Vaast	Pre-Neanderthal	France	Middle Pleistocene	7	11	11	5	3	Original data
Atapuerca-Sima de los Huesos		Spain		12	42	16	17	30	Martín-Francés et al., 2020 and original data
Visogliano		Italy				5			Zanolli et al., 2018
Ehringsdorf		Germany		7–5e	1	1			Original data from NESPOS website
Krapina	Neanderthal	Croatia	Late Pleistocene	5	28	28	23	3	Original data from NESPOS website
Scladina		Belgium		5	1			1	Olejniczak et al., 2008
La Quina		France		4–3	6	3	3	2	Original data from NESPOS website
Roc de Marsal		France		4–3	2	1	2		Original data from NESPOS website
Sima de las Palomas		Spain		3	3			3	Bayle et al., 2017
El Sidrón		Spain		3	7			7	Olejniczak et al., 2008
Spy		Belgium		3	4			4	Bayle et al., 2012
Engis (Schmerling Caves)		Belgium		3	1		1		Original data from NESPOS website
Le Moustier		France		3–2	1			1	Olejniczak et al., 2008
Wezmeh		Iran		3–2		1			Zanolli et al., 2019
Qafzeh	Fossil *H. sapiens*	Israel		5b–5	2	1	2	2	Zanolli et al., 2019
	Modern *H. sapiens*	Sudan	Holocene	1	16	15	9	7	Original data
		Europe			90	85	90	79	Olejniczak et al., 2008; Martín-Francés et al., 2020 and original data
		China			9			9	Original data

and Neanderthals from Krapina (NESPOS website) and modern humans, and published estimates for Neanderthals (Bayle et al. 2012, 2017; Olejniczak et al. 2008; Zanolli et al. 2019); fossil *H. sapiens* from Qafzeh (Zanolli et al. 2019) and modern humans (Olejniczak et al. 2008) (Table 10).

Enamel thickness topographic distribution

Three-dimensional topographic maps were generated by using the surface distance (between the enamel and dentine) module (SDM) in Amira (6.3.0, FEI Inc.). The computed distances between the OES and the EDJ are defined by a chromatic scale from thinnest (blue) to thickest (red) (Bayle et al. 2017; Macchiarelli et al. 2013). In addition to the BSV sample, we selected a sample exhibiting minimal enamel wear, including Atapuerca *H. antecessor* and SH, Neanderthals from Krapina and La Quina as well as modern humans. For representation purposes, left premolars and molars were mirror-imaged.

Geometric morphometrics of the EDJ

Geometric morphometric (GM) analyses of the EDJ were performed on the virtual surfaces of an original sample including BSV, SH, Neanderthals (NESPOS website) and modern humans (Table 1). Regarding BSV sample, those teeth exhibiting large dentine patches, such as the left P^3, were excluded from the analysis. We selected the right BSV teeth due to less dental wear. When necessary, we performed

Table 2 Mesio-distal (MD) and bucco-lingual (BL) dimensions, the crown index (CI: BLx100/MD) and the total computed crown area (TCBA: MD x BL) of the BSV teeth

Tooth	MD	BL	CI	TCBA
Left I^2	8.3	8.3	100.0	68.9
Right P^3	8.2	10.3	125.6	84.5
Left P^3	8.5	10.7	130.5	87.7
Right P^4	7.9	10.6	134.2	83.7
Left P^4	8.0	10.8	135.0	86.4
Right M^1	11.7	12.5	106.8	146.2
Left M^1	11.7	12.4	105.9	145.1
Right M^2	11.0	12.0	109.1	132.0
Left M^2	11.3	12.0	106.2	135.6
Right M^3	9.6	11.5	119.8	110.4
Left M^3	10.3	11.8	114.5	121.5

Table 3 Relative occlusal polygon area (ROPA) in BSV right molar (in bold) and comparative sample (*TD6*, *H. antecessor*; *SH*, Sima de los Huesos; *NEA*, Neanderthals; *MP HSAP*, Middle Palaeolithic *H. sapiens*; *UP HSAP*, European Upper Palaeolithic *H. sapiens*; *HSAP*, contemporary *H. sapiens*)

Sample	*N*	ROPA (%)
[a]BSV	**1**	**24.0**
[b]TD6	1	25.7
[b]SH	12	25.7 ±4.2
[c]NEA	17	26.7 ±1.8
[c]HSAP	24	37.5 ±5.4
[c]MP HSAP	4	33.3 ±2.7
[c]UP HSAP	5	32.7 ±1.9

[a]BSV: this study; [b]TD6, SH: Martinón-Torres et al., 2013; [c]NEA, MP HSAP, UP HSAP, HSAP: Bailey 2004

minimal dentine reconstruction, using the filling-holes tool in Geomagic (3D Systems, Inc.). Finally, we mirrored the comparative specimens according to the BSV teeth.

For the premolars, we placed one landmark on each of the dentine horn tips of the P^3 and P^4 (protocone and metacone) and 49 semilandmarks along the marginal ridges (SI Fig. 1A). For the M^1, we placed landmarks on the four cusps: protocone, paracone, metacone and hypocone. However, due to variability in the cusp number in M^2 and M^3, we placed landmarks on the protocone, paracone and metacone. In addition, we placed 95 semilandmarks along the marginal ridges of all molars (M^1, M^2 and M^3; see SI Fig. 1B and C). We performed the weighted between-group principal component analysis (bgPCA) based on the Procrustes and deformation-based shape residuals (Mitteroecker and Bookstein 2011) but see Bookstein (2019) and Cardini et al. (2019) for a revision of the bgPCA analysis. Finally, we tested for allometry on the landmark-based analyses using the coefficient of determination (R^2) of a multiple regression (Bookstein, 1991), in which the independent variable is centroid size and the dependent variables are the bgPC scores (Mitteroecker et al. 2013).

Statistical analyses

For representation purposes, we computed standard boxplots of the three enamel thickness variables, including AET, RET and percentage of dentine and pulp. Due to the small BSV sample size, we performed adjusted *Z*-score, comparing individually each specimen against the SH, Neanderthal and modern human groups. The adjusted *Z*-score test (Maureille et al. 2001; Scolan et al. 2012) allows the comparison of unbalanced and reduced samples (one specimen against a group) by using Student's inverse *t* distribution. Adjusted *Z*-scores of AET, RET and percentage of dentine variables were computed to compare 3D dental tissue proportions and enamel thickness values of the BSV specimens to the means and standard deviations of the SH, Neanderthal and MH groups. In these *Z*-scores, the −1.0 to +1.0 interval comprises the 95% of the variation in the reference samples.

Results

Metrics

Tables 5 and 6 present the MD and BL dimensions of the right BSV teeth. The MD and BL dimensions of BSV right

Table 4 Cusp angles in BSV right molar (in bold) and comparative sample (*TD6*, *H. antecessor*; *SH*, Sima de los Huesos; *NEA*, Neanderthals; *MP HSAP*, Middle Palaeolithic *H. sapiens*; *UP HSAP*, European Upper Palaeolithic *H. sapiens*; *HSAP*, contemporary *H. sapiens*)

Sample	*N*		A (protocone)	B (paracone)	C (metacone)	D (hypocone)
[a]BSV	**1**	**24.0**	**106.3**	**78.8**	**102.7**	**69.6**
[b]TD6	1	25.7	107.8	74.5	106	71.3
[b]SH	12/10	25.7 ±4.2	109.4 ± 8.2	73.0 ± 8.9	11.5 ±6.2	66.2 ± 5.9
[c]NEA	17	26.7 ±1.8	106.1 ± 5.2	66.7 ± 6.7	118.0 ± 10.0	69.0 ± 6.1
[c]HSAP	24	37.5 ±5.4	101.4 ± 10.1	74.3 ± 4.5	106.2 ± 5.5	78.6 ± 7.7
[c]MP HSAP	4	33.3 ±2.7	109 ± 4.5	72.5 ± 2.5	102.0 ± 1.9	79.6 ± 6.1
[c]UP HSAP	5	32.7 ±1.9	106.3 ± 4.4	71.1 ± 2.7	110.3 ± 4.9	73.3 ± 4.8

[a]BSV: this study; [b]TD6, SH: Martinón-Torres et al., 2013; [c]NEA, MP HSAP, UP HSAP, HSAP: Bailey 2004

Table 5 MD diameter of BSV (in bold, right antimere, except for the I^2) and comparative sample with descriptive statistic (*N*, number of specimens; *X*, mean value; *SD*, standard deviation) of three Pleistocene hominin samples (*SH*, Sima de los Huesos; *NEA*, Neanderthals and Krapina)

Tooth	[a]BSV	[b]SH			[c]Arago			[b]NEA			[d]Krapina		
		N	*X*	SD	*N*	*X*	SD	*N*	*X*	SD	*N*	*X*	SD
I^2	**8.3**	17	7.77	0.33	3	8.1	0.2	14	7.8	0.6	13	8.4	0.5
P^3	**8.2**	14	7.91	0.50	2	8.7		19	7.4	0.6	9	8.5	0.4
P^4	**7.9**	16	7.60	0.54	1	8.6		20	7.1	0.5	11	8.1	0.6
M^1	**11.7**	17	11.07	0.67	3	11.8	1.1	22	11.1	0.8	9	12.4	0.7
M^2	**11.0**	18	9.92	0.89	3	12.0	0.6	19	10.5	0.8	10	11.3	1.1
M^3	**9.6**	19	8.65	0.56	2	9.6		16	9.6	0.7	9	10.4	0.6

[a]BSV: this study; [b]SH, NEA: Bermúdez de Castro et al., 1993, 1999; [c]Arago: Bermúdez de Castro et al., 2019; [d]Krapina: Wolpoff, 1979

Table 6 BL diameter of the BSV (in bold, right antimere, except for the I^2) and comparative sample with descriptive statistic (*N*, number of specimens; *X*, mean value; *SD*, standard deviation) of three Pleistocene hominin samples (*SH*, Sima de los Huesos; *NEA*, Neanderthals and Krapina)

Tooth	[a]BSV	[b]SH			[c]Arago			[b]NEA			[d]Krapina		
		N	*X*	SD	*N*	*X*	SD	*N*	*X*	SD	*N*	*X*	SD
I^2	**8.3**	18	7.75	0.28	3	8.6	0.3	15	8.3	0.5	13	8.9	0.6
P^3	**10.3**	14	10.48	0.62	2	11.4	-	19	10.4	0.6	9	11.2	0.5
P^4	**10.6**	16	10.44	0.59	1	11.4	-	20	9.9	0.6	11	10.9	0.4
M^1	**12.5**	17	11.54	0.71	3	13.4	1.0	22	11.9	0.4	9	12.6	0.9
M^2	**12.0**	18	12.16	0.75	3	14.5	1.4	19	12.3	1.2	10	12.8	0.8
M^3	**11.5**	19	11.49	0.89	2	12.3	-	16	12.0	1.0	9	12.5	0.6

[a]BSV: this study; [b]SH, NEA: Bermúdez de Castro et al., 1993, 1999; [c]Arago: Bermúdez de Castro et al., 2019; [d]Krapina: Wolpoff, 1979

Table 7 Crown index (CI: BLx100/MD) in BSV (in bold, right antimere, except for the I^2) and comparative sample with descriptive statistic (*N*, number of specimens; *X*, mean value; *SD*, standard deviation) of three Pleistocene hominin samples (*SH*, Sima de los Huesos; *NEA*, Neanderthals and Krapina)

Tooth	[a]BSV	[b]SH			[c]Arago			[b]NEA			[d]Krapina		
		N	*X*	SD	*N*	*X*	SD	*N*	*X*	SD	*N*	*X*	SD
I^2	**100**	17	100.06	2.88	3	105.46	6.83	14	106.38	7.32	13	106.27	10.18
P^3	**125.61**	14	133.44	4.05	2	131.60	-	19	140.00	10.02	9	131.50	5.41
P^4	**134.17**	16	137.50	4.98	1	132.56	-	20	141.24	6.49	11	135.16	7.78
M^1	**106.84**	17	104.36	6.06	3	113.42	3.49	22	107.32	8.03	9	101.51	3.10
M^2	**109.09**	18	122.60	7.29	3	120.71	8.71	19	117.37	12.18	10	114.53	8.52
M^3	**119.79**	19	133.08	8.76	2	128.12	-	16	125.83	9.73	9	120.80	5.28

[a]BSV: this study; [b]SH, NEA: Bermúdez de Castro et al., 1993, 1999; [c]Arago: Bermúdez de Castro et al., 2019; [d]Krapina: Wolpoff, 1979

Table 8 Total computed crown base area (TCBA) in BSV (in bold, right antimere, except for the I^2) and comparative sample with descriptive statistic (*N*, number of specimens; *X*, mean value; *SD*, standard deviation) of three Pleistocene hominin samples (*SH*, Sima de los Huesos; *NEA*, Neanderthals and Krapina)

Tooth	[a]BSV	[b]SH			[c]Arago			[b]NEA			[d]Krapina		
		N	*X*	SD	*N*	*X*	SD	*N*	*X*	SD	*N*	*X*	SD
I^2	**68.9**	17	60.43	4.52	3	69.63	1.43	14	64.00	8.93	13	74.83	6.46
P^3	**84.5**	14	83.61	9.76	2	99.84	-	19	78.00	9.11	9	95.90	8.34
P^4	**83.7**	16	79.70	10.04	1	98.04	-	20	70.90	9.44	11	88.55	9.67
M^1	**146.2**	17	128.09	14.04	3	158.48	57.08	22	131.93	11.14	9	156.13	19.98
M^2	**132.0**	18	121.20	17.31	3	175.31	24.88	19	129.55	18.19	10	144.92	21.45
M^3	**121.5**	19	99.96	12.72	2	118.08	-	16	114.84	15.61	9	130.25	12.00

[a]BSV: this study; [b]SH, NEA: Bermúdez de Castro et al., 1993, 1999; [c]Arago: Bermúdez de Castro et al., 2019; [d]Krapina: Wolpoff, 1979

Table 9 Frequencies of the degrees of expression of main morphological traits in BSV and comparative samples. *BSV*, Biache-Saint-Vaast; *SH*, Sima de los Huesos; *MP*, European Middle Pleistocene from Visogliano; *NEA*, Neanderthals; *FHS*, fossil *H. sapiens*; *MH*, modern humans (see Table SI 1 for the individual scoring of each specimen)

I^2	Grade	[1]BSV	[1]SH	[2]MP	[1,2]NEA	[2]FHS	[1]MH
Labial convexity	0						4 (66.67%)
	1						
	2						
	3						2 (33.33%)
	4	1 (100%)			2 (33.33%)		
	5		3 (100%)		4 (66.67%)		
	6						
	Total	1	3		6		6
Shovel shape	0						1 (16.66%)
	1						
	2						2 (33.33%)
	3		2 (66.67%)		1 (16.66%)		1 (16.66%)
	4				1 (16.66%)		
	5	1 (100%)	1 (33.33%)		3 (50%)		1 (16.66%)
	6				1 (16.66%)		1 (16.66%)
	Total	1	3		6		6
Tuberculum dentale	0				1 (16.66%)		3 (50%)
	1						
	2						
	3		1 (33.33%)				
	4		1 (33.33%)				
	5						2 (33.33%)
	6	1 (100%)	1 (33.33%)		5 (83.33%)		1 (16.66%)
	Total	1	3		6		6
P^3	Grade	BSV	SH	MP	NEA	FHS	MH
Premolar distal accessory ridge	0	2 (100%)	1 (33.3%)		3 (60%)		4 (50%)
	1		2 (66.6%)		2 (40%)		4 (50%)
	Total	2	3		5		8
Premolar mesial accessory ridge	0	2 (100%)	2 (66.7%)		4 (80%)		5 (62.5%)
	1		1 (33.3%)		1 (20%)		3 (37.5%)
	Total	2	3		5		8
Transverse crest of premolars	0		2 (66.7%)		1 (20%)		6 (75%)
	1	1(50%)			1 (20%)		2 (25%)
	2	1 (50%)	1 (33.3%)	2 (100%)	3 (60%)		
	Total	2	3	2	5		8
Buccal essential crest or ridge	0						
	1	1(50%)	2 (66.7%)		3 (60%)		8 (100%)
	2	1 (50%)	1 (33.3%)		2 (40%)		
	Total	2	3		5		8
Lingual essential crest or ridge	0		1 (33.3%)				2 (25%)
	1	1(50%)	1 (33.3%)		3 (60%)		6 (75%)
	2	1 (50%)	1 (33.3%)		2 (40%)		
	Total	2	3		5		8
P^4	Grade	BSV	SH	MP	NEA	FHS	MH
Premolar distal accessory ridge	0	1 (100%)	1 (50%)		2 (66.7%)		4 (26.67%)
	1		1 (50%)	1 (100%)	1 (33.3%)		11 (73.33%)
	Total	1	2	1	3		15

Table 9 (continued)

I^2	Grade	[1]BSV	[1]SH	[2]MP	[1,2]NEA	[2]FHS	[1]MH
Premolar mesial accessory ridge	0	1 (100%)	2 (100%)		3 (100%)		6 (40%)
	1			1 (100%)			9 (60%)
	Total	1	2	1	3		15
Transverse crest of premolars	0		1 (50%)				10 (66.67%)
	1		1 (50%)	0	1 (33.3%)		2 (13.33%)
	2	1 (100%)		1 (100%)	2 (66.7%)		3 (20%)
	Total	1	2	1	3		15
Buccal essential crest or ridge	0						1 (6.66%)
	1		2 (100%)		1 (33.3%)		14 (93.24%)
	2	1 (100%)		1 (100%)	2 (66.7%)		
	Total	1	2	1	3		15
Lingual essential crest or ridge	0						7 (46.62%)
	1	1 (100%)		1 (100%)	1 (33.3%)		7 (46.62%)
	2		2 (100%)		2 (66.7%)		1 (6.67%)
	Total	1	2	1	3		15
M^1	Grade	BSV	SH	MP	NEA	FHS	MH
Crista	0						
obliqua	1	1 (100%)	2 (100%)	1 (100%)	4 (100%)	1 (100%)	9 (100%)
	Total	1	2	1	4	1	9
Transverse crest	0	1 (100%)	1 (50%)	1 (100%)	2 (50%)		8 (88.9%)
	1		1 (50%)		2 (50%)	1 (100%)	1 (11.1%)
	Total	1	2	1	4	1	9
Carabelli	0		1 (50%)				1 (11.11%)
	1						2 (22.22%)
	2		1 (50%)				1 (11.11%)
	3				1 (25%)		2 (22.22%)
	4			1 (100%)	2 (50%)		2 (22.22%)
	5						1 (11.11%)
	6	1 (100%)					
	7				1 (25%)	1 (100%)	
	Total	1	2	1	4	1	9
Parastyle	0		2 (100%)	1 (100%)	4 (100%)	1 (100%)	9 (100%)
	1	1 (100%)					
	2						
	3						
	4						
	5						
	6						
	Total	1	2	1	4	1	9
Mesial marginal accessory tubercles	0	1 (100%)		1 (100%)	2 (50%)	1 (100%)	8 (88.9%)
	1		2 (100%)		2 (50%)		1 (11.1%)
	Total	1	2	1	4	1	9
Metacone (C3)	0						
	1						
	2						
	3						
	4	1 (100%)	2 (100%)	1 (100%)	4 (100%)	1 (100%)	8 (88.9%)
	5						1 (11.1%)
	Total	1	2	1	4	1	9

Table 9 (continued)

I^2	Grade	[1]BSV	[1]SH	[2]MP	[1,2]NEA	[2]FHS	[1]MH
Hypocone (C4)	0						
	1						
	2				0	0	
	3						
	4		1 (50%)	1 (100%)	0	1 (100%)	6 (66.67%)
	5	1 (100%)	1 (50%)		4 (100%)		3 (33.33%)
	Total	1	2	1	4	1	9
Metaconule (C5)	0	1 (100%)	2 (100%)	1 (100%)	3 (75%)		7 (77.8%)
	1						
	2				1 (25%)		1 (11.1%)
	3					1 (100%)	1 (11.1%)
	4						
	5						
	Total	1	2	1	4	1	9
M^2	Grade	BSV	SH	MP	NEA	FHS	MH
Crista obliqua	0						4 (16.6%)
	1	1 (100%)	3 (100%)	1 (100%)	7 (100%)		20 (83.4%)
	Total	1	3	1	7		24
Transverse crest	0	1 (100%)	3 (100%)	1 (100%)	2 (28.6%)		22 (91.7%)
	1	1			5 (71.4%)		2 (8.3%)
	Total		3	1	7		24
Carabelli	0		3 (100%)		3 (42.8%)		20 (83.3%)
	1						1 (4.2%)
	2						1 (4.2%)
	3		0	1 (100%)	3 (42.8%)		2 (8.3%)
	4	1 (100%)			1 (14.4%)		
	5						
	6						
	7						
	Total	1	3	1	7		24
Parastyle	0	1 (100%)	3 (100%)	1 (100%)	7 (100%)		24 (100%)
	1						
	2						
	3						
	4						
	5						
	6						
	Total	1	3	1	7		24
Mesial marginal accessory tubercles	0	1 (100%)	3 (100%)	1 (100%)	6 (85.7%)		18 (75%)
	1				1 (14.3%)		6 (25%)
	Total	1	3	1	7		
Metacone (C3)	0						
	1						
	2						
	3						
	4	1 (100%)	3 (100%)		5 (71.4%)		14 (58.3%)
	5			1 (100%)	2 (28.6%)		10 (41.7%)
	Total	1	3	1	7		24

Table 9 (continued)

I^2	Grade	[1]BSV	[1]SH	[2]MP	[1,2]NEA	[2]FHS	[1]MH
Hypocone (C4)	0						3 (12.5%)
	1						
	2		1 (33.3%)				
	3	1 (100%)	2 (66.7%)	1 (100%)	1 (14.3%)		9 (37.5%)
	4				1 (14.3%)		9 (37.5%)
	5				5 (71.4%)		3 (12.5%)
	Total	1	3	1	7		24
Metaconule (C5)	0	1 (100%)		1 (100%)	7 (100%)		23 (95.9%)
	1						
	2		1 (33.3%)				1 (4.1%)
	3		2 (66.7%)				
	4						
	5						
	Total	1	3	1	7		24
M^3	Grade	BSV	SH	MP	NEA	FHS	MH
Crista obliqua	0	1 (100%)	3 (100%)		5 (55.6%)		21 (55.3%)
	1				4 (44.4%)		17 (44.7%)
	Total	1	3		9		38
Transverse crest	0	1 (100%)	3 (100%)		5 (55.6%)		34 (89.5%)
	1				4 (44.4%)		4 (10.5%)
	Total	1	3		9		38
Carabelli	0	1 (100%)	3 (100%)		6 (66.7%)		27 (71.1%)
	1						
	2						1 (2.6%)
	3				1 (11.1%)		2 (5.3%)
	4				2 (22.2%)		4 (10.5%)
	5						1 (2.6%)
	6						2 (5.3%)
	7						1 (2.6%)
	Total	1	3		9		38
Parastyle	0	1 (100%)	3 (100%)		9 (100%)		38 (100%)
	1						
	2						
	3						
	4						
	5						
	6						
	Total	1	3		9		34
Mesial marginal accessory tubercles	0		3 (100%)		3 (33.3%)		31 (81.6%)
	1	1 (100%)			6 (66.7%)		7 (18.4%)
	Total	1	3		9		38
Metacone (C3)	0						
	1						
	2		1 (33.3%)				
	3	1 (100%)	2 (66.7%)				1 (2.7%)
	4				8 (88.9%)		14 (36.8%)
	5				1 (11.1%)		23 (60.5%)
	Total	1	3		9		38

Table 9 (continued)

I^2	Grade	[1]BSV	[1]SH	[2]MP	[1,2]NEA	[2]FHS	[1]MH
Hypocone (C4)	0		2 (66.7%)				9 (23.7%)
	1						
	2		1 (33.3%)				3 (7.9%)
	3	1 (100%)			6 (66.7%)		20 (52.6%)
	4				2 (22.2%)		6 (15.8%)
	5				1 (11.1%)		
	Total	1	3		9		38
Metaconule (C5)	0	1 (100%)	3 (100%)		5 (55.6%)		30 (79%)
	1						
	2				2 (22.2%)		1 (2.3%)
	3				2 (22.2%)		5 (13.3%)
	4						2 (5.4%)
	5						
	Total	1	3		9		38

[1]BSV, SH, NEA and MH: this study; [2]MP and FHS from Zanolli et al. 2018 and NEA from Wezmeh Zanolli et al. 2019

teeth are higher than the main values obtained for the SH and Neanderthal samples (Bermúdez de Castro 1993), except for the Krapina population (Wolpoff 1979). In contrast, Arago dental samples have larger MD and BL dimensions compared to BSV, SH and most Neanderthal specimens (Bermúdez de Castro 1993; Bermúdez de Castro et al. 1999, 2019).

The low CI values estimated for BSV (Table 7) dental remains are closer to the mean value of SH sample than to any other group, except for the right M^2 and M^3 that are closer to Krapina mean values (Bermúdez de Castro et al. 1993, 1999, 2019; Wolpoff 1979).

The ROPA of the BSV right M^1 represents the 24.0% of the TCBA (Tables 3 and 8). This value is within the variation range of SH population (Martinón-Torres et al. 2013) and Neanderthals (Bailey 2004) and out of the range of variation reported for early and contemporary *H. sapiens* (Bailey 2004). As for the cusp angles (Table 4), BSV right M^1 follows the pattern A > C > B > D, which is the pattern described for *H. antecessor* (Martinón-Torres et al. 2013).

Morphological characterisation of the OES and EDJ

Following, we will describe the main morphological traits observed in the BSV teeth, OES and EDJ, as well as its comparison with the rest of the sample. A detailed description of the OES and EDJ morphology of the BSV and comparative sample can be found in SI and SI Tables S1–S3.

Overall, we observed that BSV displays the so-called typical Neanderthal morphology, in both the presence and degree of expression of traits. In addition, we found a good correspondence between the BSV OES and EDJ surfaces, although in some instances the expression of features in the EDJ is higher than what we observed in the OES. As such, we only included in the description those EDJ features that did not show correspondence with those observed in the OES (Table 9 for the frequencies of the degree of expression of main morphological traits in BSV and comparative samples).

Left I^2 (Figs. 1 and 2) exhibits a wear category of 3–4 (Molnar's classification, 1971). At the OES, this tooth shows a pronounced labial convexity, strong shovel shape and tuberculum dentale with a free apex. This suite of traits is commonly observed in SH, Neanderthals and Arago compared to modern humans (Martinón-Torres et al. 2012; Zanolli et al. 2018).

Right and left P^3s (Figs. 1 and 3) exhibit wear categories 2 and 3 (Molnar 1971), respectively. While the right P^3 exhibits a single buccal and lingual essential ridges, these are bifurcated in the left P^3, morphologies frequently seen in SH and Neanderthals (Martinón-Torres et al. 2012). Moreover, the left P^3 presents a continuous transverse crest, a trait commonly recorded in MP samples (Zanolli et al. 2018).

Right and left P^4s (Figs. 1 and 4) exhibit wear category 2 (Molnar 1971). We recorded a continuous transverse crest as well as a single buccal and a bifurcated lingual essential crest in the right P^4. In the left P^4, the essential crests are bifurcated, a common trait recorded in MP hominins (Zanolli et al. 2018), but not in SH (Martinón-Torres) and Neanderthals (Martinón-Torres et al. 2012).

Right and left M^1s (Figs. 1 and 5) exhibit wear category 3 (Molnar 1971). The bulging and well-developed hypocone is responsible for the distobuccal protrusion of the crown in

Table 10 3D enamel thickness variables assessed in BSV P^4, M^2 and M^3 (in bold) and the comparative sample including extinct and extant specimens/populations

Sample	*N*	Tooth class		3D AET (mm)	3D RET	Vcdp/Vc (%)
		UP4				
[a]BSV	**1**			**1.07**	**18.81**	**52.23**
[b]HER	1			1.13	19.30	55.06
[c]SH	7		Mean	1.09	20.71	50.05
			SD	0.08	2.21	2.88
			Range	0.97–1.23	18.75–24.07	46.63–54.06
[d]NEA	6		Mean	1.15	20.96	50.91
			SD	0.19	2.15	2.34
			Range	0.82–1.34	17.87–23.55	47.98–53.54
[e]FHS	2		Mean	1.19	23.32	48.23
			SD	0.06	0.19	0.88
			Range	1.14–1.23	23.18–23.44	47.56–48.81
[f]MH	21		Mean	1.25	25.17	46.19
			SD	0.17	3.89	3.93
			Range	0.98–1.52	17.28–31.78	39.65–54.64
		UM2				
[g]BSV	**1**			**1.37**	**21.05**	**49.58**
[h]SH	8		Mean	1.24	20.15	51.51
			SD	0.10	1.47	1.64
			Range	1.05–1.43	18.43–23.74	48.24–54.14
[i]NEA	6		Mean	1.10	15.91	58.18
			SD	0.13	2.94	4.48
			Range	0.97–1.33	13.24–20.88	50.70–62.80
[j]MH	28		Mean	1.37	22.79	49.88
			SD	0.18	3.53	3.45
			Range	0.96–1.78	15.06–31.63	43.24–58.46
		UM3				
[k]BSV	**1**			**1.39**	**23.33**	**46.78**
[l]HER	1			1.45	27.64	42.45
[m]SH	14		Mean	1.36	25.39	46.10
			SD	0.11	2.06	2.08
			Range	1.18–1.50	21.24–30.02	41.43–50.82
[n]NEA	9		Mean	1.03	15.62	58.47
			SD	0.14	2.05	3.54
			Range	0.75–1.18	11.61–18.43	54.06–66.11
[o]MH	46		Mean	1.52	27.18	45.80
			SD	0.23	4.68	4.18
			Range	0.91–1.94	14.54–35.28	37.83–53.77

P^4: [a]BSV1: this study; [b]HER: *H. erectus* (Zhoukoudian PA68 original data); [c]SH: Sima de los Huesos (AT-5510, AT-746, AT-2189, AT-2070, AT-559, AT-5836, AT-221 original data); [d]NEA: Neanderthals (Krapina: D42, D44, D117 and La Quina 18 Martín-Francés et al., submitted; Las Palomas: SP68 and SP94 Bayle et al., 2017), [e]FH: fossil *H. sapiens* (Qafzeh: 10 and 15 Zanolli et al., 2019); [f]MH: modern humans (original data). M^2: [g]BSV1: this study; [h]SH: Sima de los Huesos (AT-12, AT-824, AT-817, AT-15, AT-170, AT-960, AT-822, AT-2175, AT-6215); [i]NEA: Neanderthals (El Sidrón: SR332, SR4, SR531, SR551 Olejniczak et al., 2008; Spy I Bayle et al., 2012 and La Quina 18 original data); [j]MH: modern humans (Martín-Francés et al., 2020 and original data). M^3: [k]BSV1: this study; [l]HER: *H. erectus* (Sangiran NG0802.1 Zanolli, 2015); [m]SH: Sima de los Huesos (AT-10, AT-194, AT-601, AT-805, AT-826, AT-3181, AT-1471, AT-2393, AT-3183; AT-5082, AT-5292, AT-274, AT-602, AT-6215 original data); [n]NEA: Neanderthals (El Sidrón: SR407, SR741, SR621; Le Moustier: 1; Scladina: 4A_3 Olejniczak et al., 2008; Spy I, I and II Bayle et al., 2012; Las Palomas: SP51 Bayle et al., 2017); [o]MH: modern humans (Martín-Francés et al., 2020 and original data)

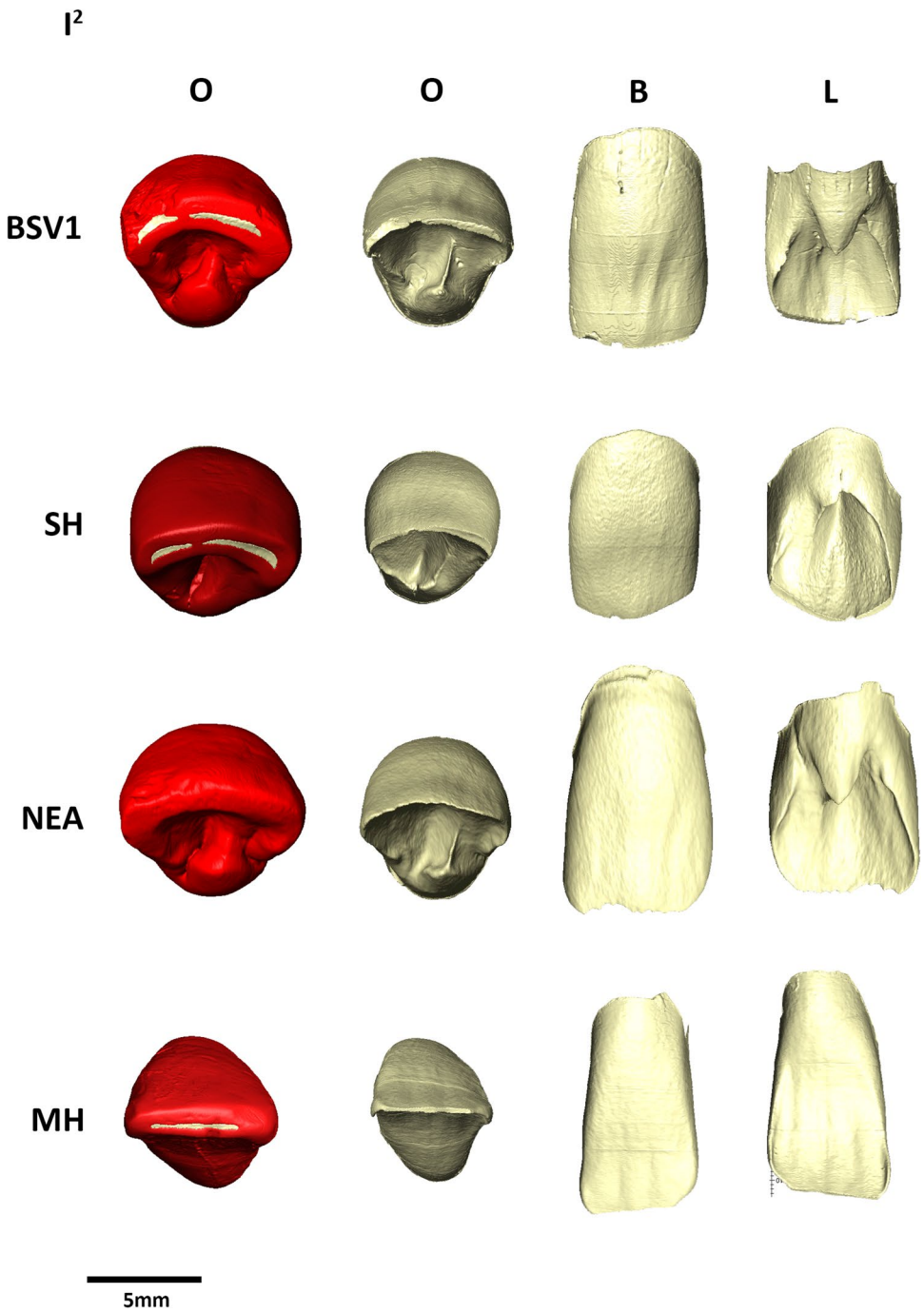

Fig. 2 3D reconstruction of the I^2 outer enamel surface (OES) and enamel-dentine junction (EDJ) views in BSV1 compared to those of Sima de los Huesos, Neanderthal and modern human. SH = Sima de los Huesos (AT-1753), NEA = Neanderthal (Ehringsdorf G3), MH = modern human (UCL91). O = occlusal, B = buccal, L = lingual. (When needed, specimens have been mirrored to the right to match the BSV1 specimen)

both M^1s, a configuration widely recorded in MP samples as well as Neanderthals (Gómez-Robles et a. 2007). The high degree of expression of the Carabelli complex recorded in BSV M^1s, even more conspicuous on the EDJ than on the OES, is only surpassed by Neanderthals.

Right and left M²s (Figs. 1 and 6) exhibit wear category 2 (Molnar 1971). Both M^2s are characterised by the reduction of the hypocone area, resulting from the shortening of the distal rim in comparison to the mesial one, a conformation commonly recorded in the MP populations, including SH and Visogliano (Martinón-Torres et al., 2012; Zanolli et al. 2018).

Right and left M³s (Figs. 1 and 7) are unworn (category 1; Molnar 1971). The occlusal contour is a rounded trapezoid, with narrowing of the talonid resulting from the reduced hypocone. This conformation is in common in MP hominins and Neanderthals (Martinón-Torres et al., 2012). At the EDJ level, we observed the presence of marginal tubercles in both M^3s, a trait not recorded in the OES.

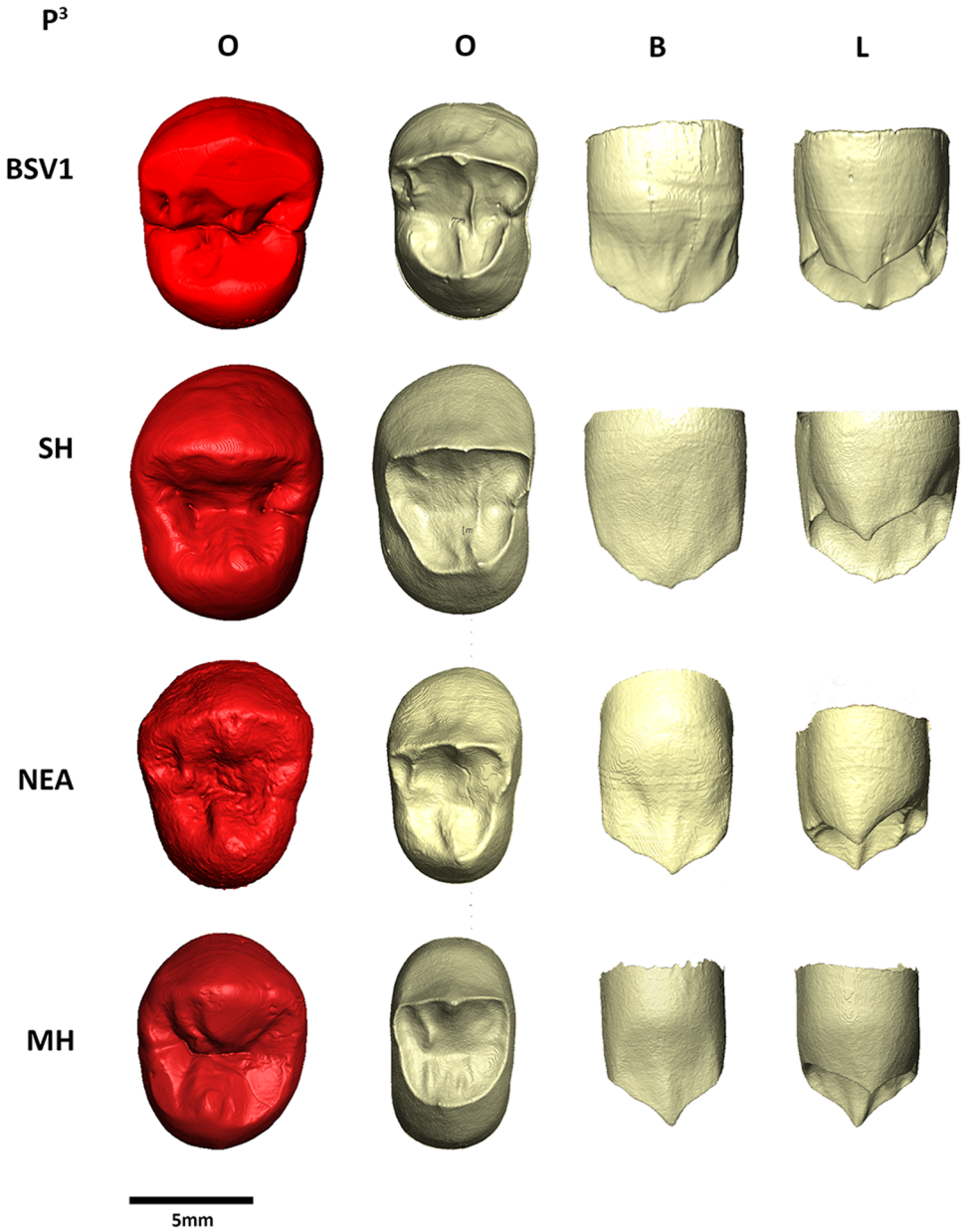

Fig. 3 3D reconstruction of the P^3 outer enamel surface (OES) and enamel-dentine junction (EDJ) views in BSV1 compared to those of Sima de los Huesos, Neanderthal and modern human. SH = Sima de los Huesos (AT-2399), NEA = Neanderthal (La Quina), MH = modern human (UCL20). O = occlusal, B = buccal, L = lingual. (When needed, specimens have been mirrored to the right to match the BSV1 specimen)

Enamel thickness

3D estimates of enamel thickness and crown tissue proportions of BSV1 specimens are described in Table 6 together with the mean, S.D. and range values of the comparative samples. Overall, BSV1 individual exhibits a mixed pattern characterised by thinly enamelled premolars and thickly enamelled molars (Fig. 8).

Although BSV1 right P^4 values for absolute and relative enamel thickness (AET and RET) are within the range of variation of all comparative samples, the BSV1 P^4 shows the lowest absolute and relative (AET and RET) values of enamel thickness in relation to the mean values of the comparative sample. BSV1 P^4 aligns with SH and Neanderthal samples for the AET, RET and Vcdp/Vc and discriminates from both the fossil *H. sapiens* and modern humans (Table 10).

BSV1 M^2 and M^3 show high values of AET and RET similar to the mean values of Atapuerca populations (TD6 and SH; Martín-Francés et al. 2018; Martín-Francés et al. 2020). The BSV estimated values for AET, RET and Vcdp/Vc are within the range of variation of TD6, SH and modern human groups and outside the Neanderthal variation range. These results emphasise the affinity of BSV with SH and its departure from the Neanderthal condition (Table 10).

Although BSV right P^4 falls within the 95% of variation range of all comparative groups, the BSV specimen closer resembles the Neanderthal thin condition, shared also with

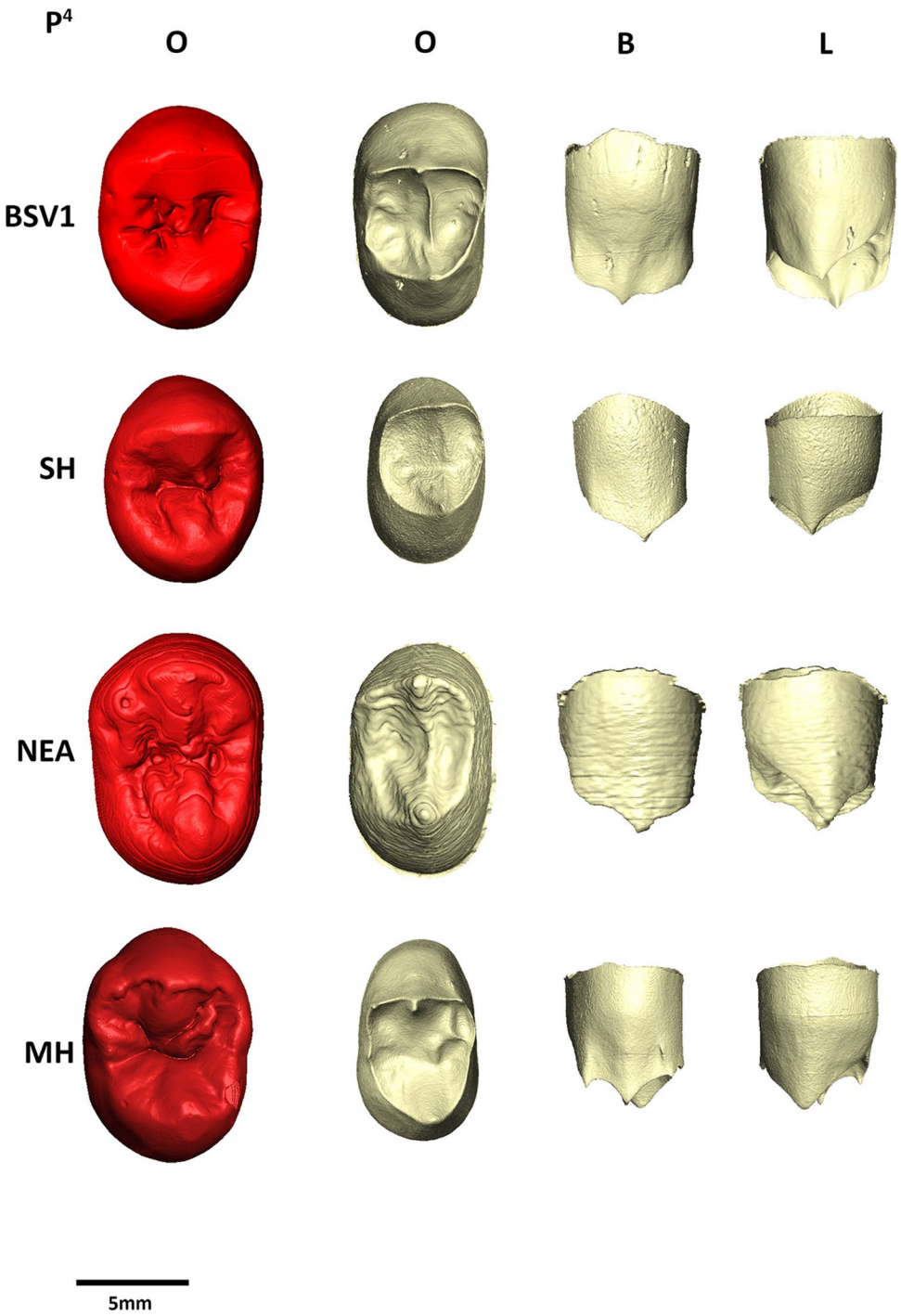

Fig. 4 3D reconstruction of the P^4 outer enamel surface (OES) and enamel-dentine junction (EDJ) views in BSV1 compared to those of Sima de los Huesos, Neanderthal and modern human. SH = Sima de los Huesos (AT-5510), NEA = Neanderthal (Krapina D42), MH = modern human (UCL62). O = occlusal, B = buccal, L = lingual. (When needed, specimens have been mirrored to the right to match the BSV1 specimen)

SH, and differentiates it from the modern human thick condition (Fig. 9). The BSV right M^2 closer resembles the modern human condition although the values for the AET, RET and Vcdp/Vc fall within the 95% of variation range of all comparative groups. The BSV1 right M^3 shows closer affinity with SH sample, thick condition, for all three variables, although BSV also falls within the 95% of modern human variation range. On the contrary, the BSV1 right M^3 clearly departs from the Neanderthal condition as it falls outside the 95% of the variation range.

Enamel thickness distribution

Overall, BSV1 dental remains show closer affinity with the pattern of enamel distribution shown by SH specimens (Figs. 10, 11 and 12).

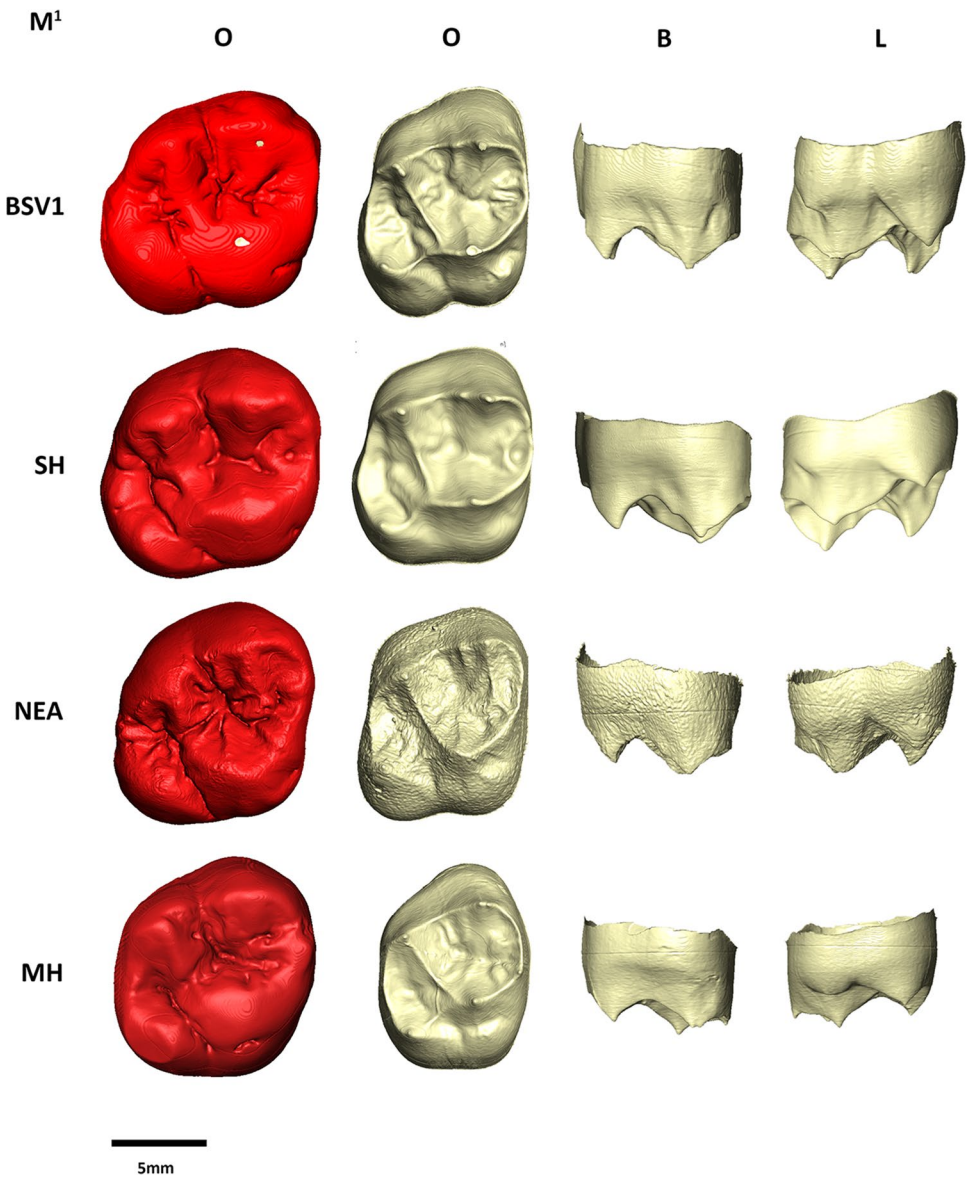

Fig. 5 3D reconstruction of the M^1 outer enamel surface (OES) and enamel-dentine junction (EDJ) views in BSV1 compared to those of Sima de los Huesos, Neanderthal and modern human. SH = Sima de los Huesos (AT-2071), NEA = Neanderthal (Krapina D101), MH = modern human (UCM76). O = occlusal, B = buccal, L = lingual. (When needed, specimens have been mirrored to the right to match the BSV1 specimen)

The pattern of enamel thickness distribution in the peripheral areas, mostly on the buccal and lingual surfaces of the two main cusps, is observed in BSV1, TD6, SH and Neanderthal specimens, and different from the modern human specimen showing thicker enamel on the occlusal basin (Fig. 10).

Although the wear exhibited by the BSV1 M^2 may conceal some aspects of the enamel distribution, in general BSV shares with SH and modern human specimen the larger areas of enamel thickness on the buccal and the lingual surface of the cusps. In TD6, the enamel is thicker and more widespread in these areas, while in Neanderthals, the thickness is more subtle in bucco-lingual cusps (Fig. 11).

BSV1 M^3 shares with the modern human specimen thicker enamel distributed in the lingual cusp (protocone) as well as in the two buccal cusps and the occlusal basin. The distribution exhibited by SH specimen also resembles this. In contrast, in the Neanderthal specimen thickness is more peripherally distributed (Fig. 12).

Geometric morphometrics

The results of the bgPCA analyses of the BSV specimens are shown in Figs. 13, 14, 15, 16 and 17.

Figure 13 illustrates the bgPCA analysis for the BSV1 right P^3. The two principal components account for the 99.14% of the total variation. BSV1 specimen shares the negative PC1 morphospace with SH and Neanderthal specimens characterised by a more round-shaped outline conferred by the shorter M-D diameter. Similarly, BSV specimen clusters with all SH specimens, and few Neanderthal

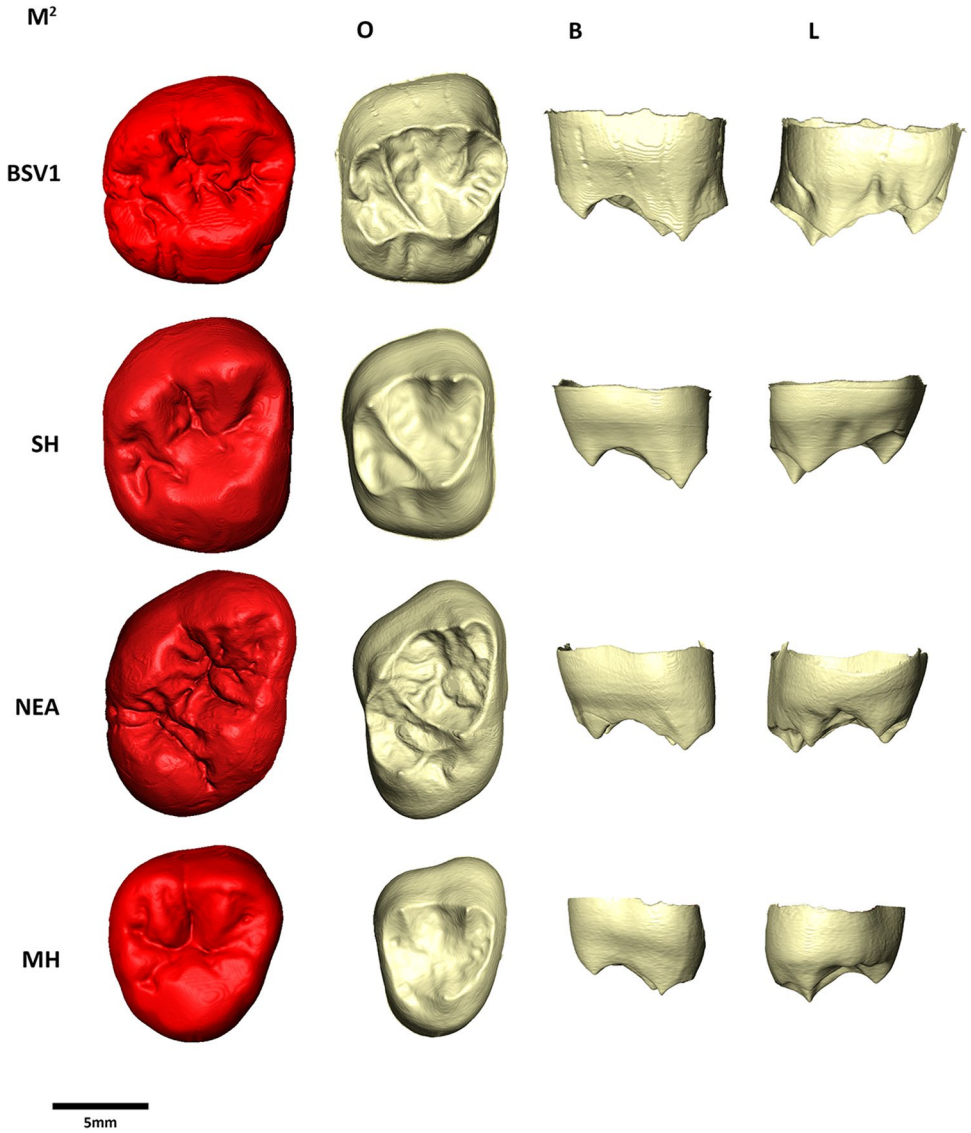

Fig. 6 3D reconstruction of the M^2 outer enamel surface (OES) and enamel-dentine junction (EDJ) views in BSV1 compared to those of Sima de los Huesos, Neanderthal and modern human. SH = Sima de los Huesos (AT-960), NEA = Neanderthal (La Quina), MH = modern human (MI). O = occlusal, B = buccal, L = lingual. (When needed, specimens have been mirrored to the right to match the BSV1 specimen)

and modern human specimens, on the positive axis of the PC2, characterised by rounded, versus a rectangular, outline.

In the bgPCA analysis of BSV1 right P^4 (Fig. 14), the two principal components account for the 98.97% of the total variation, with the PC1 accounting for the 89.78%. BSV1 shares the morphospace with SH specimens and half of modern humans, characterised by a more rounded-shaped outline, with slightly larger mesio-distal diameter, and the protocone and paracone slightly distally placed in comparison to Neanderthals and the rest of the modern human sample.

Figure 15 illustrates the bgPCA analysis for the BSV1 right M^1. The two principal components account for the 84.26% of the total variation. BSV1 specimen shares the positive PC1 morphospace with the two specimens from SH and the majority of Neanderthals characterised by a rectangular outline conferred by the larger area of the distal cusps, specially the distally placed hypocone, and the shorter height of the dentine horns, in contrast to the fossil *H. sapiens* and modern human samples.

The results of the bgPCA analysis of the BSV1 right M^2 is shown in Fig. 16. The two principal components account for the 99.78% of the total variation. BSV1 specimen falls within the positive PC1 together with SH specimens and half of the modern human sample. These are characterised by a more squared-shaped outline consequence of hypocone reduction, and in contrast to the Neanderthal morphology characterised by a rectangular-shaped outline resulting from a distally displaced and protruding hypocone.

Figure 17 illustrates the bgPCA for the right M^3. The two principal components account for the 99.92% of the total variation. BSV1 specimen shares the positive morphospaces with SH specimens, three Neanderthals from Krapina and some modern human specimens. These are characterised by

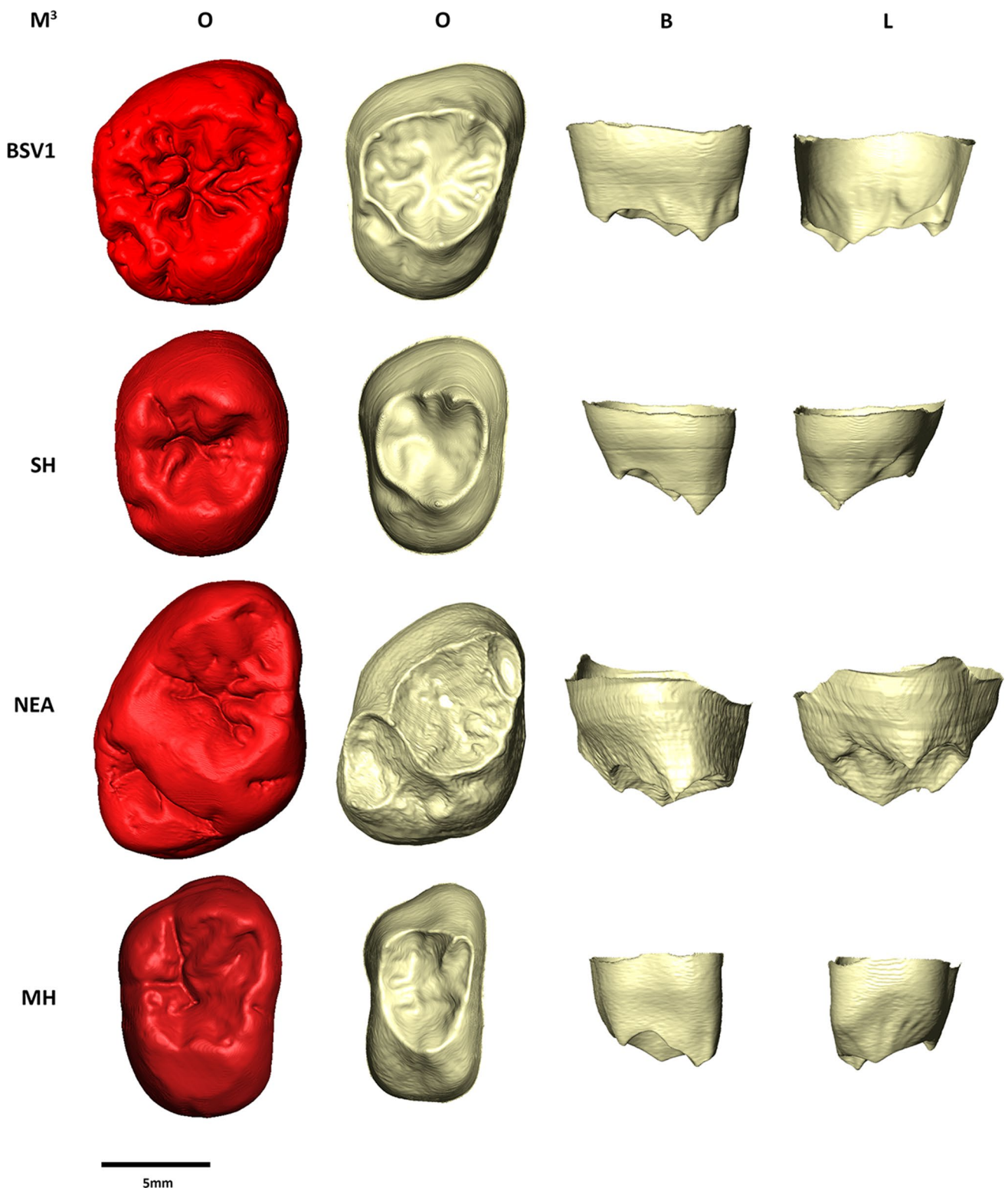

Fig. 7 3D reconstruction of the M^3 outer enamel surface (OES) and enamel-dentine junction (EDJ) views in BSV1 compared to those of Sima de los Huesos, Neanderthal and modern human. SH = Sima de los Huesos (AT-1471), NEA = Neanderthal (Krapina D178), MH = modern human (CR72). O = occlusal, B = buccal, L = lingual. (When needed, specimens have been mirrored to the right to match the BSV1 specimen)

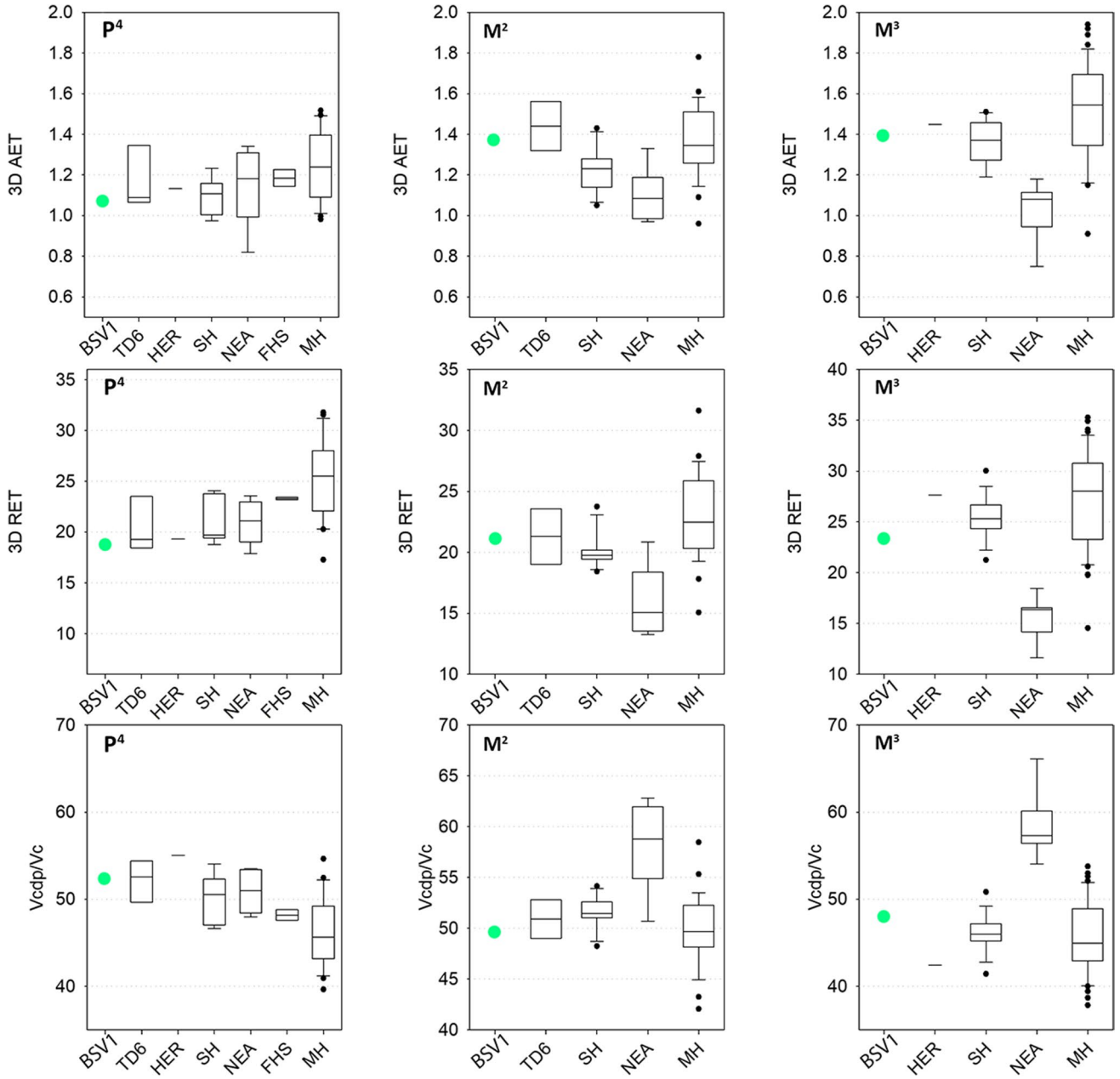

Fig. 8 Box plots of the 3D crown values. 3D values depicting the average enamel thickness (3D AET), relative enamel thickness (3DLRET) and the percentage of dentine and pulp in the crown (Vcdp/Vc), in the maxillary P^4, M^2 and $M^3$of the BSV and the comparative specimens/samples

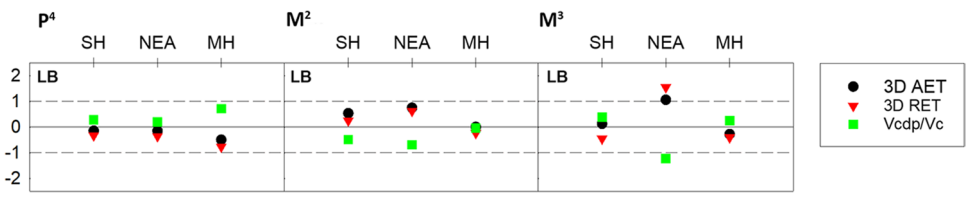

Fig. 9 Adjusted *Z*-score of the 3D variables: AET (black circles), RET (red triangles) and percentage of dentine (green squares) assessed in P^4, M^2 and M^3 from BSV and compared to the variation expressed by Sima de los Huesos (SH), Neanderthals (NEA) and modern humans (MH). The solid line passing through zero represents the mean, and the other two lines correspond to the estimated 95% limit of variation expressed for the two comparative samples

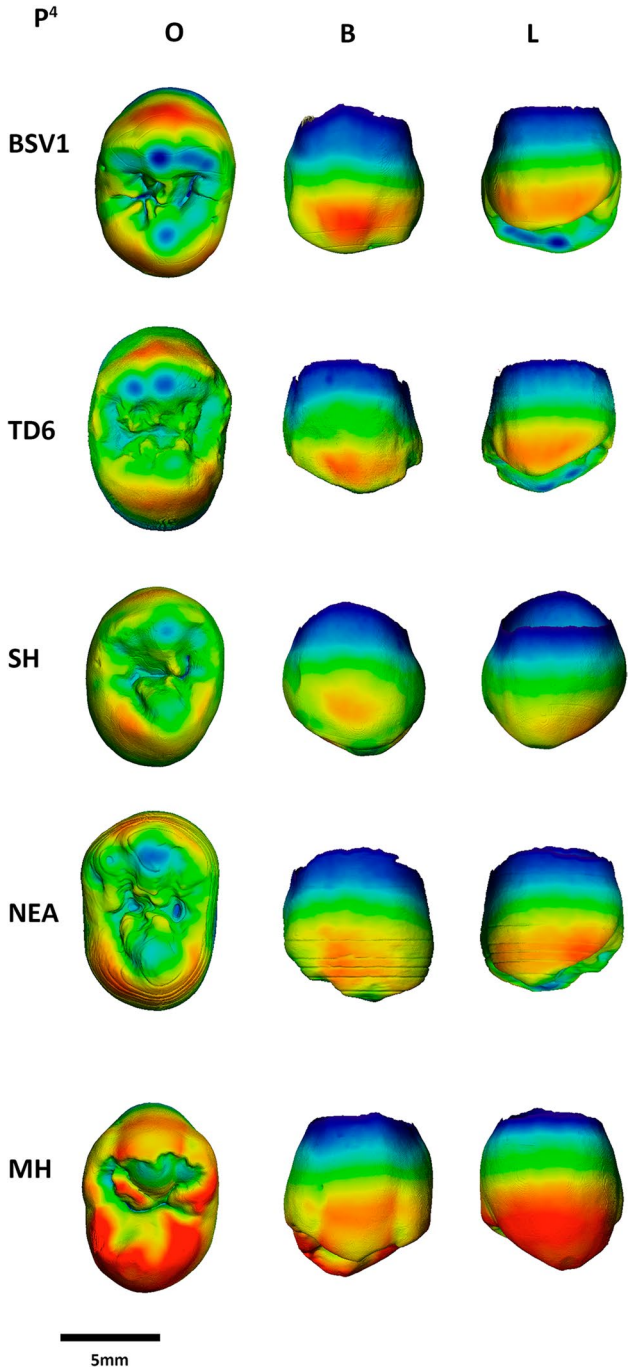

Fig. 10 Enamel thickness cartographies of the BSV P^4 compared with those of *H. antecessor*, Sima de los Huesos, Neanderthal and modern human. Topographic thickness variation is rendered by a pseudo-colour scale ranging from thinner dark-blue to thicker red. TD6 = *H. antecessor* (TD6-8), SH = Sima de los Huesos (AT-5510), NEA = Neanderthal (Krapina D42) and MH = modern human (UCL62). O = occlusal, B = buccal, L = lingual. (When needed, specimens have been mirrored to the left to match the SH specimen)

an oval-shaped outline elongated on bucco-lingual direction resulting from the more distally placed protocone and the reduction of the hypocone, in contrast to the rest of the Neanderthal sample and majority of modern human specimens.

In all cases, Pearson correlation test for allometry showed a weak signal (P^3 $p<0.05$, $R^2=0.13$; P^4 $p<0.05$, $R^2=0.302$; M^1 $p<0.05$, $R^2=0.20$; UM^3 $p<0.05$, $R^2=0.00$), except for the M^2 that shows moderate allometry ($p<0.05$, $R^2=0.44$).

Discussion

In the last years, the discovery of new fossils as well as the reassessment of old findings is providing evidence of the high morphometric variation of the European populations during the MP, where populations with different geographic and chronological settings present different Neanderthal affinities. In this context, the variability of the MP populations could be better explained by less linear models such as the ebb and flow model (Hublin and Roebroeks 2009) or the sink and source model (Bermúdez de Castro and Martinón-Torres 2013; Dennell et al. 2011). While in the ebb and flow model human groups retreated to refugia when conditions worsened, the alternative sink and source model suggests a pattern of repeated colonisation and extinction but also hybridization had occurred. Population hybridization would have sustained the interpopulation variability through time (Bermúdez de Castro and Martinón-Torres 2013; Dennell et al. 2011). In this context, studies noted differences in the suite of Neanderthal dental features between MP populations and suggested the possibility of coexistence of several paleodemes during this time in Europe (e.g. Bermúdez de Castro et al. 2019; Martínez de Pinillos et al. 2020; Zanolli et al. 2018). One group would cluster specimens that are lacking Neanderthal apomorphies in their dentitions such as Mala Balanica (BH-1), Mauer or Arago (e.g. Bailey 2002; Bermúdez de Castro et al. 2019; Gómez-Robles et al. 2007, 2011; Roksandic 2016; Skinner et al. 2016). While, the second group would be characterised by closer morphological dental affinities with the classic Neanderthals, including the Atapuerca-SH, Pontnewydd, Fontana Ranuccio, Visogliano, Steinheim and Montmaurin hominins (e.g. Gómez-Robles et al. 2007, 2011; Hanegraef et al. 2018; Martínez de Pinillos et al. 2020; Martinón-Torres et al. 2012; Zanolli et al. 2018). However, even within these groups there is variability. While Mauer and Mala Balanica hominins lack the thin enamel pattern characteristic of Neanderthals (Skinner et al. 2016; Smith et al. 2012), the Arago dentition exhibits thin enamelled crowns (Macchiarelli et al. 2013). Similarly, Fontana Ranuccio, Visogliano and Steinheim exhibit the enamel thickness pattern typical of Neanderthals, but Atapuerca-SH and Montmaurin molars are characterised by thick enamelled crowns.

Previous assessments of the BSV crania remains assigned these hominins to a population between late *H.*

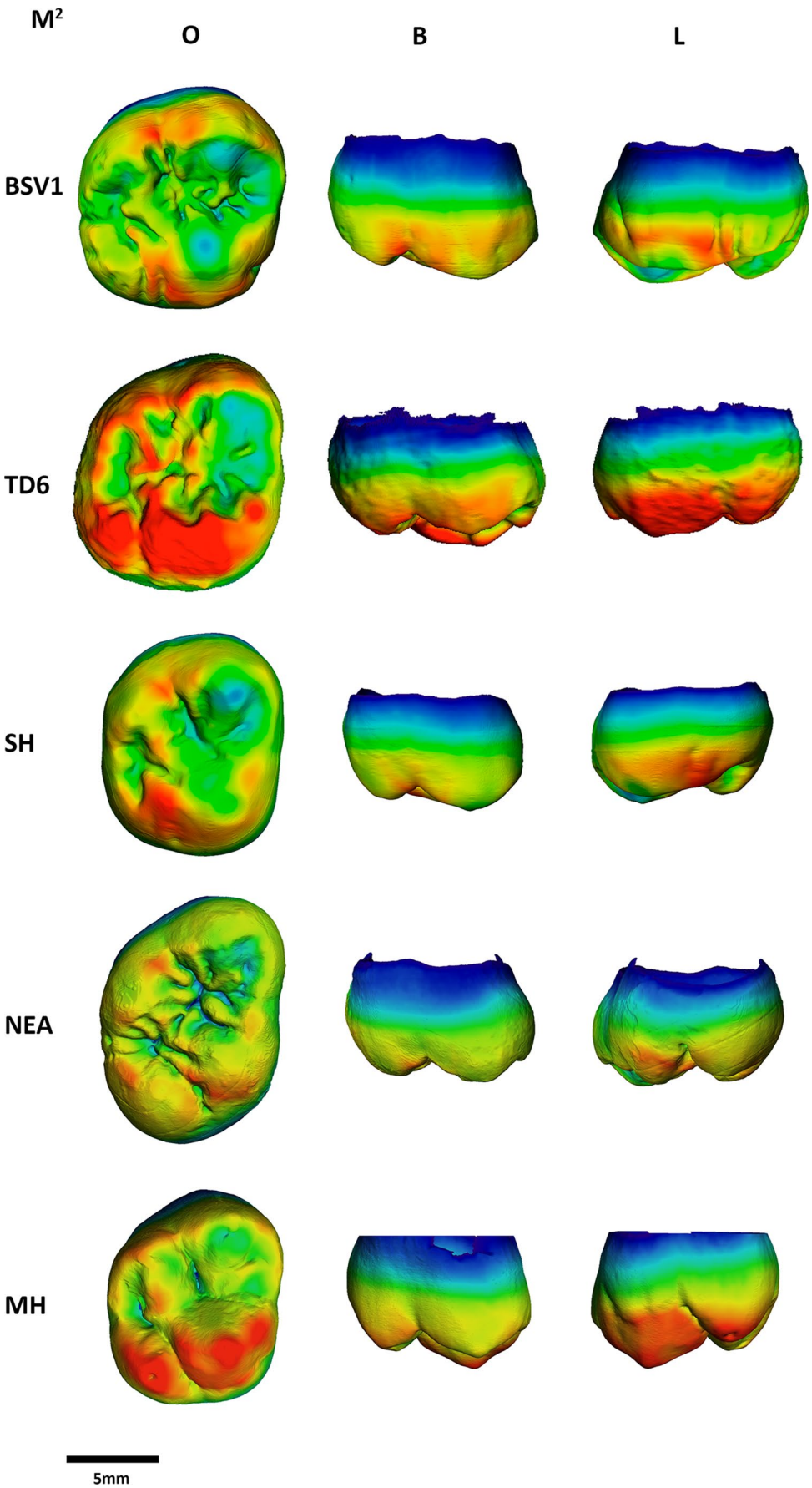

Fig. 11 Enamel thickness cartographies of the BSV M^2 compared with those of *H. antecessor*, Sima de los Huesos, Neanderthal and modern human. Topographic thickness variation is rendered by a pseudo-colour scale ranging from thinner dark-blue to thicker red. TD6 = *H. antecessor* (TD6-69), SH = Sima de los Huesos (AT-960), NEA = Neanderthal (La Quina) and MH = modern human (MI). O = occlusal, B = buccal, L = lingual. (When needed, specimens have been mirrored to the left to match the SH specimen)

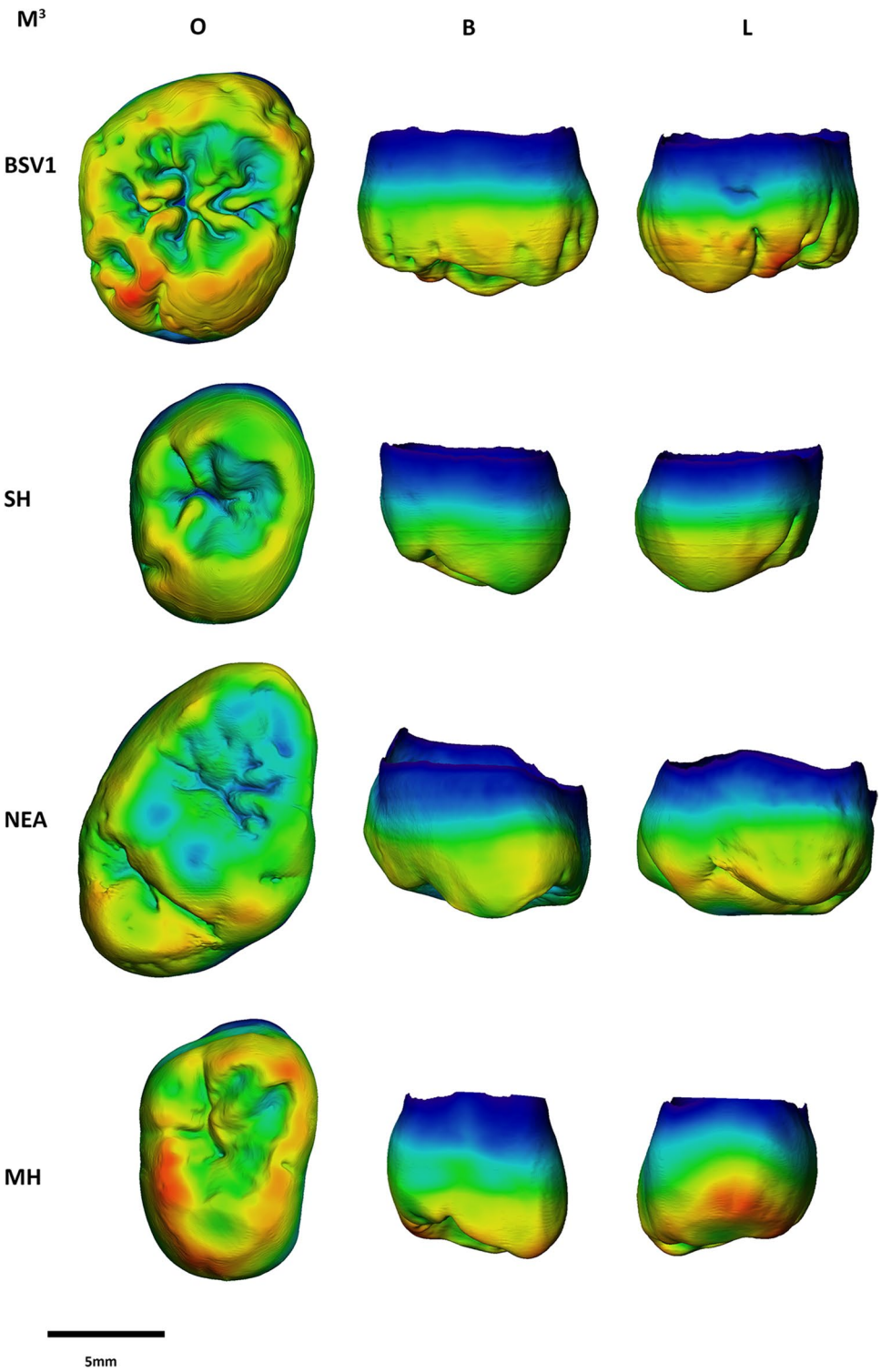

Fig. 12 Enamel thickness cartographies of the BSV M^3 compared with those of Sima de los Huesos, Neanderthal and modern human. Topographic thickness variation is rendered by a pseudo-colour scale ranging from thinner dark-blue to thicker red. SH = Sima de los Huesos (AT-1471), NEA = Neanderthal (Krapina D178) and MH = modern human (CR72). O = occlusal, B = buccal, L = lingual. (When needed, specimens have been mirrored to the left to match the SH specimen)

heidelbergensis and the first *H. neanderthalensis* (Vandermeersch, 1978, 1982; Rougier, 2003). Arsuaga and Martínez (1997) analysis of the temporal bone of BSV2 concluded that this individual closely resembled the morphology of the "Neanderthal 1" group than those of the European MP. Finally, Guipert et al. (2011) concluded that BSV2 individual belonged to the first European Neanderthals due to the combination of Neanderthal apomorphies and several plesiomorphies. Within this scenario, the study of BSV fossil teeth aims to explore the BSV affinities with other MP groups and Neanderthals as well as contributing to the discussion about the MP population variability.

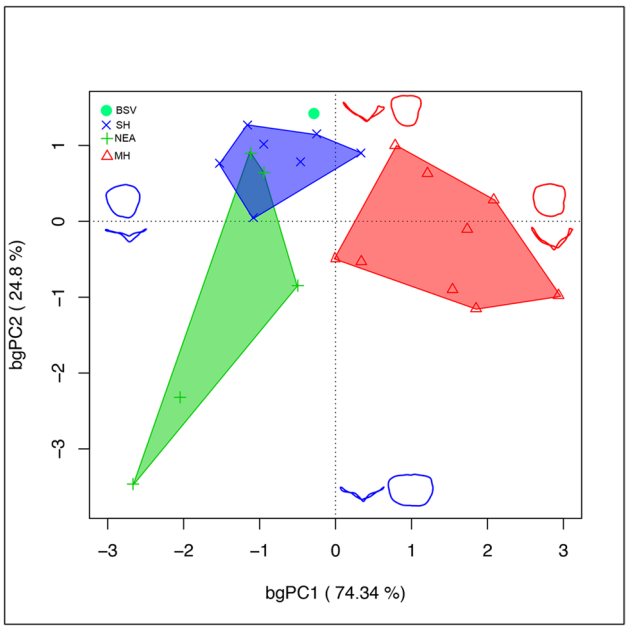

Fig. 13 Between-group principal component analysis (bgPCA) of the Procrustes shape coordinates of the BSV1 P^3 EDJ compared with those of Sima de los Huesos (SH), Neanderthals (NEA) and modern humans (MH)

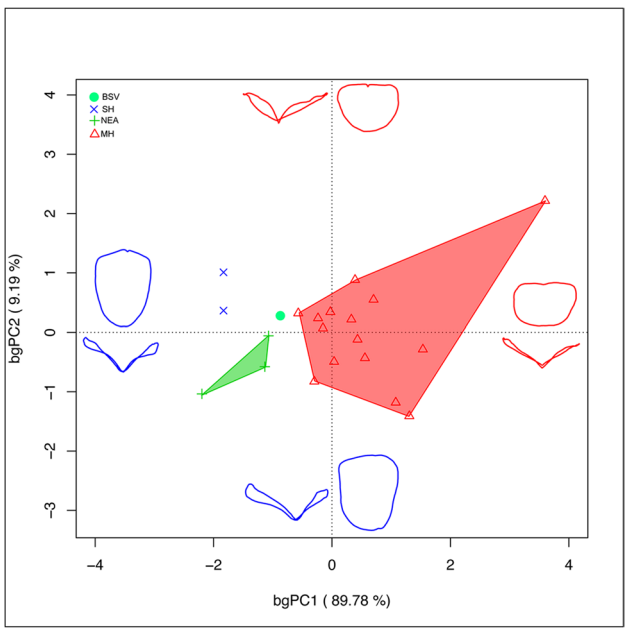

Fig. 14 Between-group principal component analysis (bgPCA) of the Procrustes shape coordinates of the BSV1 P^4 EDJ compared with those of Sima de los Huesos (SH), Neanderthals (NEA) and modern humans (MH)

Previous metric data such as the CI, ROPA, TCBA, cusp angles or enamel thickness confirmed the differences between Neanderthals and *H. sapiens* (e.g., Bailey 2004; Bermúdez de Castro 1993; Buti et al. 2017; Martinón-Torres et al. 2013; Olejniczak et al. 2008). In this study, the performed metric analyses resulted in BSV showing greater affinities with SH and Neanderthals than with any other group for all variables except the cusp angles. BSV right M^1 shares the pattern with *H. antecessor* species (Martinón-Torres et al. 2013), thus displaying a less Neanderthal-like condition than SH but more derived than in *H. erectus*. Similarly, the enamel thickness pattern shown by BSV dental remains, combination of thin enamel in the premolars and thick enamel in the molars, is exclusively shared with the MP population from SH. We can tentatively relate the enamel thickness similarities between BSV and SH to their morphometric similarities; however, enamel thickness variation results from the interplay of multiple factors, including genetic (Horvath et al. 2014), developmental and life history features (Dean et al. 2001; Grine 2002, 2005; Smith et al. 2007), the structural organisation of the mineralized dental tissues (Macchiarelli et al. 2006; Olejniczak et al. 2008), dental and body size reduction (Kupczik and Hublin 2010; Lieberman 2011; Smith et al. 2012) and dietary adaptions (Lucas et al. 2008; Olejniczak et al. 2008), that should also be explored. Regarding the external (OES) and internal (EDJ) morphology, BSV exhibits a suite of features characteristic of some MP populations (including SH, Pontnewydd and Vigliano) as well as Neanderthals (e.g. Bailey 2004, 2006; Martinón-Torres et al. 2012; Zanolli et al. 2018, 2019). The concomitant expression in the I^2 of a marked shovel shape, a pronounced labial convexity and a well-developed tuberculum dentale represents the typical Neanderthal morphology. The M^1s have a characteristic morphology, in which the occlusal contour is rhomboidal, with a distal displacement of the lingual cusps and a rounded protrusion of the distobuccal corner due to a large hypocone. In particular, this morphology was already present in the Early Pleistocene hominins from the Gran Dolina-TD6 site (Gómez-Robles et al. 2007) and thus, it may represent a primitive morphology retained by some MP populations (such as SH, Pontnewydd and Steinheim but not Arago) and Neanderthals (Bermúdez de Castro et al. 2019; Compton and Stringer 2015; Gómez-Robles et al. 2007). Although previous studies showed the limited morphological discrimination of the premolars between Neanderthals and *H. sapiens* (e.g. Martinón-Torres et al. 2019; Zanolli et al. 2019), the BSV premolars display some features that are prevalent in MP hominins and Neanderthals but quite uncommon in modern humans. As such, the presence of a transverse crest and lingual essential crest in the BSV P^3s and P^4s is also expressed in other MP populations (such as SH and Visogliano), and the majority of Neanderthals (including the recently described specimen from Wezhem) but its presence is quite limited in the modern human sample (Martinón-Torres et al. 2012; Zanolli et al. 2018, 2019; and this study). Even though

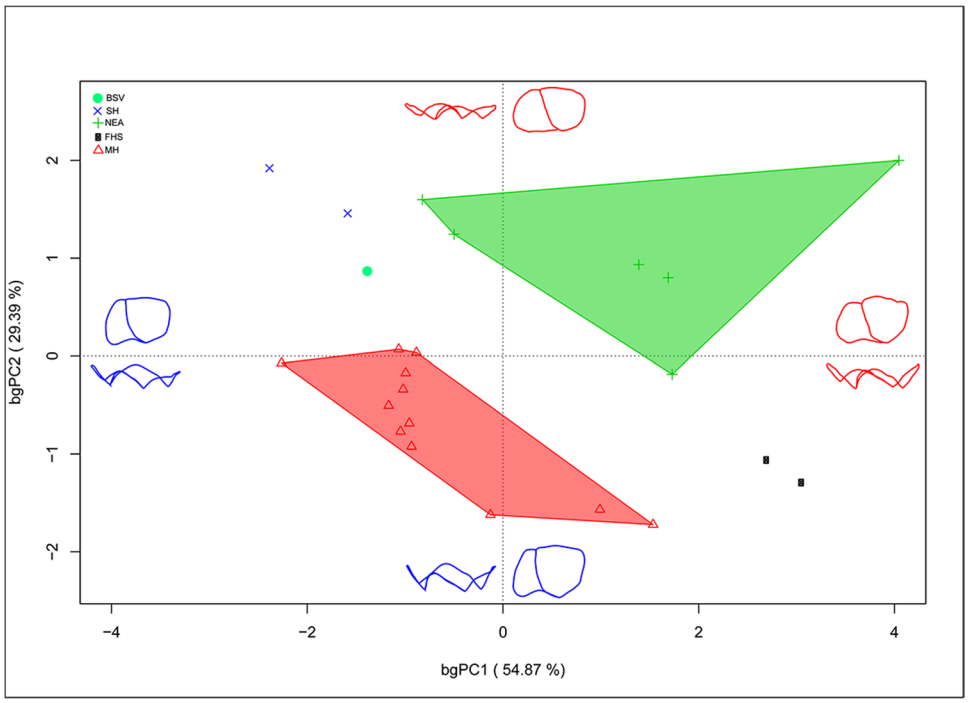

Fig. 15 Between-group principal component analysis (bgPCA) of the Procrustes shape coordinates of the BSV1 M^1 EDJ compared with those of Sima de los Huesos (SH), Neanderthals (NEA), fossil *H. sapiens* (FHS) and modern humans (MH)

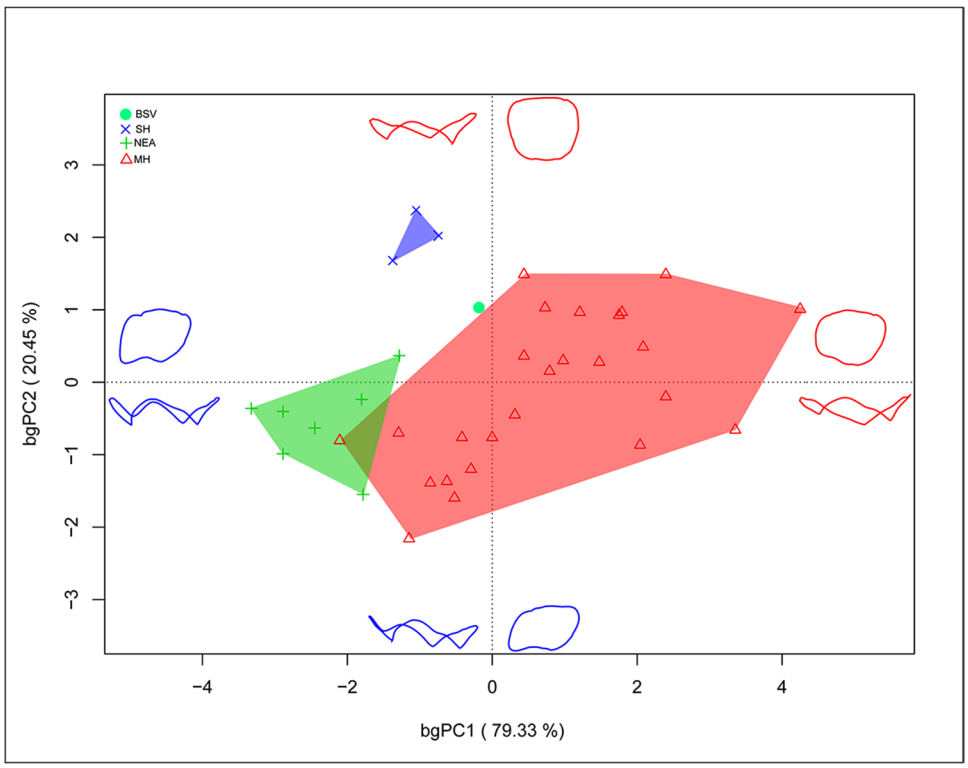

Fig. 16 Between-group principal component analysis (bgPCA) of the Procrustes shape coordinates of the BSV1 M^2 EDJ compared with those of Sima de los Huesos (SH), Neanderthals (NEA) and modern humans (MH)

the BSV M^2 and M^3 do not display any diagnostic feature shared exclusively with MP hominins and Neanderthals, the GM analysis of the EDJ shape contour in these molars, as well as in the premolars, shows that BSV dental remains share greater affinities with the MP sample from SH and modern humans than with Neanderthals. In particular, at the EDJ, the degree of reduction of the metacone and the hypocone in M^2 and M^3 aligns BSV with SH hominins and modern humans. Thus, the morphometric analysis of BSV dentition places these hominins within the MP group that

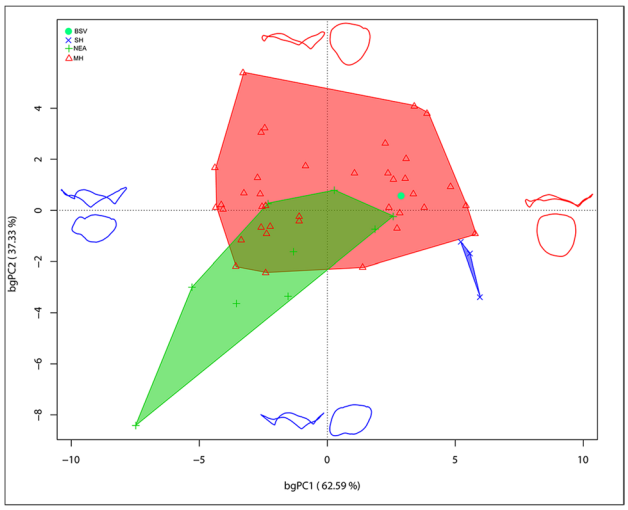

Fig. 17 Between-group principal component analysis (bgPCA) of the Procrustes shape coordinates of the BSV1 M^3 EDJ compared with those of Sima de los Huesos (SH), Neanderthals (NEA) and modern humans (MH)

exhibits more Neanderthal affinities in their dentitions, in particular, closer to the SH population due to the expression of the morphological traits, EDJ shape and enamel thickness. Still, and despite the younger chronology of the BSV hominins with respect to SH, in some instances BSV dental remains do not exhibit the derived condition for some traits that are indeed present in SH population. For instance, BSV exhibits the primitive condition for the cusp angle trait, following the pattern described for *H. antecessor*, while both SH and Neanderthals exhibit the derived condition.

When studying MP populations, one of the greatest challenges comes from the scarcity of the fossil record, which is mainly represented by isolated remains that are geographically and chronologically scattered. For decades, the discussion on the origin of the Neanderthal clade was dominated by the accretion theoretical model. This model explains the neanderthalization process as the gradual accumulation of Neanderthal traits through time (Dean et al. 1998; Hublin 2009). However, the MP fossil record, prominently the Atapuerca-SH hominins, questioned its validity (Dennell et al. 2011; Martinón-Torres et al. 2012). Despite its early chronology, ca. 430 ka, the SH dentition is morphologically "more Neanderthal" than other penecontemporaneous MP samples and even more derived than some classic Neanderthals, thus contradicting the gradual and ordered neanderthalization process defended by the accretion model, where specimens would align from less to more Neanderthal along a chronological scale (Martinón-Torres et al. 2012). This new description of the BSV dental remains reinforces the evidence of the high morphological variation of the European populations during the MP, where populations with different geographic and chronological settings present different Neanderthal affinities. As such, based on dental analyses, two groups are recognised; the first one clusters specimens characterised by a more primitive morphology with less to none Neanderthal affinities such as Mala Balanica (BH-1), Mauer or Arago (e.g. Bailey 2002; Bermúdez de Castro et al. 2019; Gómez-Robles et al. 2007, 2011; Roksandic, 2016; Skinner et al. 2016). The second group includes those hominins exhibiting most (if not all) the dental features that are considered typical of the Neanderthal species, including the Atapuerca-SH, Pontnewydd, Fontana Ranuccio, Visogliano, Steinheim, Montmaurin and BSV hominins (e.g. Gómez-Robles et al. 2007, 2011; Hanegraef et al. 2018; Martínez de Pinillos et al. 2020; Martinón-Torres et al. 2012; Zanolli et al. 2018). However, when considering other skeletal parts we still observe intrapopulation variability within these two groups. While BSV cranial remains exhibit clear Neanderthal features, the number of primitive features retained by the SH population is higher (Rougier 2003; Arsuaga and Martínez 1997). Similarly, while SH mandibles exhibit a clear Neanderthal pattern (Rosas 2001), the Montmaurin mandible is characterised by a particularly primitive conformation (Vialet et al. 2018). The question is whether these two MP groups represent (i) a single population with a high degree of variability or (ii) two distinct paleodemes, understood as "representative of prehistoric populations or lineages acting as portions of dynamic evolutionary units" (Trinkaus 1990) where only the one with clear Neanderthal dental affinities (including SH, Pontnewydd, Fontana Ranuccio, Visogliano, Steinheim, Montmaurin and BSV) can be considered active contributors for the Neanderthal gene pool. In contrast to the linearity proposed by the accretion model, we feel that the high variability within the MP populations fits better with the sink and source model (Dennell et al. 2011), where instead of an anagenetic in situ evolution of the MP populations into Neanderthals, the settlement of Europe is seen as the result of intermittent dispersals into Europe from a source population located outside the continent. The source population would evolve in what we named as the Central Area of Dispersals of Eurasia (CADE) giving rise to daughter populations that disperse to the West and the East of Eurasia when environmental conditions allow (Bermúdez de Castro and Martinón-Torres 2013; Dennell et al. 2011). The recent publication of the Nesher Ramla fossils in the Levantine Corridor (Hershkovitz et al. 2021) would support the idea of the Near East representing the residential area of a population that was likely involved in the evolution of the MP *Homo* and Neanderthals in Europe through discontinuous migrations.

Conclusion

We examined the external and internal dental structures of the maxillary dental remains recovered from Biache-Saint-Vaast site in order to contribute to the current debate on the variability of the European MP hominins and the evolution of the Neanderthal clade. Our study shows that BSV teeth cluster with other MP groups that show greater dental affinities with Neanderthals such as Atapuerca-SH, Fontana Ranuccio, Visogliano, Steinheim and Montmaurin, and in contrast to the specimens showing less Neanderthal features, such as Arago, Mauer or Mala Balanica. Within the Neanderthal-like group, we also observed variability related to the enamel thickness variation. In this aspect, the BSV hominins are closer to the Atapuerca-SH population, than to any other group (i.e. Fontana Ranuccio, Visogliano or Steinheim), since they show a unique combination of thin (premolars) and thick (molars) enamelled dentition. The results on BSV dental remains together with previous evidence of the MP fossil record indicate the coexistence of two or more populations in Europe that may result from an intermittent settlement of human groups originated in the CADE as proposed in the sink and source model.

Supplementary Information The online version contains supplementary material available at https://doi.org/10.1007/s12520-022-01680-6.

Acknowledgements We are very grateful to Catherine Schwab, Curator at the Musée d'Archéologie Nationale in Saint-Germain-en-Laye, who welcomed us to study the BSV teeth stored under her responsibility and who facilitated the procedure to carry out the µCT acquisition. For this later step, we thank Marta Bellato at the Ast-Rx (MNHN, Paris) who kindly found the best technical solutions. The comparative samples, including SH and modern humans, were scanned at CENIEH-ICTS facilities with the collaboration of the CENIEH staff.

Funding Open Access funding provided thanks to the CRUE-CSIC agreement with Springer Nature. Partial financial support was received from the DRAC Occitanie, Ministry of Culture, France, in the context of the Montmaurin prehistoric caves project (Dir. by A. Vialet) and Project PID2021-122355NB-C33 financed by MCIN/AEI/10.13039/501100011033/ FEDER, UE. M-MT has received support from the Leakey Foundation through the personal support of Gordon Getty (2013) and Dub Crook (2014-2022). LM-F has received support from the Atapuerca Foundation, and the Spanish Ministry of Science and Innovation through the "María de Maeztu" excellence accreditation (CEX2019-000945-M) and currently from the project IJC2020-043979-I financed by the MCIN/AEI/10.13039/501100011033, and NextGenerationEU/PRTR.

References

Arsuaga JL, Martínez I (1997) The temporal bones from Sima de los Huesos middle Pleistocene site (sierra de Atapuerca, Spain). A phylogenetic approach. J Hum Evol 33:283–318

Arsuaga JL, Martínez I, Arnold LJ, Aranburu A, Gracia-Téllez A, Sharp WD, Quam RM, Falguères C, Pantoja-Pérez A, Bischoff J, Poza-Rey E, Parés JM, Carretero JM, Demuro M, Lorenzo C, Sala N, Martinón-Torres M, García N, Alcázar de Velasco A et al (2014) Neandertal roots: cranial and chronological evidence from Sima de los Huesos. Science 344:1358–1363

Bahain J-J, Falguères C, Laurent M, Dolo J-M, Shao Q, Auguste P, Tuffreau A (2015) ESR/U-series dating of faunal remains from the paleoanthropological site of Biache-saint-Vaast (Pas-de-Calais, France). Quat Geochronol 30:541–546

Bailey SE (2006) Beyond shovel-shaped incisors: Neandertal dental morphology in a comparative context. Period Biol 108:253–267

Bailey SE (2002) A closer look at Neanderthal postcanine dental morphology: the mandibular dentition. Anat Rec 269:148–156

Bailey SE (2004) A morphometric analysis of maxillary molar crowns of middle-Late Pleistocene hominins. J Hum Evoln 47:183–198

Bayle P, Le Luyer M, Robson Brown KA (2017) The Palomas dental remains: Enamel thickness and tissues proportions, in: Trinkaus, E., Walker, M.J. (Eds.), the people of Palomas: Neandertals from the Sima de las Palomas del Cabezo Gordo, Southeastern Spain. A&M University anthropology series, College Station, Texas, pp. 115–137

Bayle P, Mazurier A, Macchiarelli R (2012) The permanent « virtual dentitions » of spy I and spy II. In: Rougier H, P., S. (eds) Spy cave: 125 years of multidisciplinary research at the Betche aux Roches (Jemeppe-Sur-Sambre. Institut Royal des Sciences Naturelles de Belgique, Province de Namur, Belgium), Bruxelles

Bermúdez de Castro JM (1993) The Atapuerca dental remains: new evidence (1987-1991 excavations) and interpretations. J Hum Evol 24:339–371

Bermúdez de Castro JM, Martinón-Torres M (2013) A new model for the evolution of the human Pleistocene populations of Europe. Quat Int 295:102–113

Bermúdez de Castro JM, Martinón-Torres M, Martínez de Pinillos M, García-Campos C, Modesto-Mata M, Martín-Francés L, Arsuaga JL (2019) Metric and morphological comparison between the Arago (France) and Atapuerca-Sima de los Huesos (Spain) dental samples, and the origin of Neanderthals. Quat Sci Rev 217:45–61

Bermúdez de Castro JM, Martinón-Torres M, Rosell J, Blasco R, Arsuaga JL, Carbonell E (2016) Continuity versus discontinuity of the human settlement of Europe between the late Early Pleistocene and the early middle Pleistocene. The mandibular evidence Quat Sci Rev 153:51–62

Bermúdez de Castro JM, Rosas A, Nicolás ME (1999) Dental remains from Atapuerca-TD6 (Gran Dolina site, Burgos, Spain). J Hum Evol 37:523–566

Bookstein FL (1991) Morphometric tools for landmark data: geometry and biology. Cambridge University Press, Cambridge

Bookstein FL (2019) Pathologies of between-groups principal components analysis in geometric morphometrics. Evol Biol 46:271–302

Buti L, Le Cabec A, Panetta D, Tripodi M, Salvadori PA, Hublin J-J, Feeney RNM, Benazzi S (2017) 3D enamel thickness in Neandertal and modern human permanent canines. J Hum Evol 113:162–172

Cardini A, O'Higgins P, Rohlf FJ (2019) Seeing distinct groups where there are none: spurious pattern from between-group PCA 46:303–316

Compton T, Stringer C (2015) The morphological affinities of the middle Pleistocene hominin teeth from Pontnewydd cave, Wales. J Quat Sci 30:713–730

Daura J, Sanz M, Arsuaga JL, Hoffmann DL, Quam RM, Ortega MC, Santos E, Gómez S, Rubio A, Villaescusa L, Souto P, Mauricio J, Rodrigues F, Ferreira A, Godinho P, Trinkaus E, Zilhão J (2017) New middle Pleistocene hominin cranium from Gruta da Aroeira (Portugal). PNAS 114:3397–3402

Dean C, Leakey MG, Reid D, Schrenk F, Schwartz GT, Stringer C, Walker A (2001) Growth processes in teeth distinguish modern humans from Homo erectus and earlier hominins. Nature 414:628–631

Dean D, Hublin J-J, Holloway R, Ziegler R (1998) On the phylogenetic position of the pre-Neandertal specimen from Reilingen, Germany. J Hum Evol 34:485–508

Demuro M, Arnold LJ, Aranburu A, Sala N, Arsuaga J-L (2019) New bracketing luminescence ages constrain the Sima de los Huesos hominin fossils (Atapuerca, Spain) to MIS 12. J Hum Evol 131:76–95

Dennell RW, Martinón-Torres M, Bermúdez de Castro JM (2011) Hominin variability, climatic instability and population demography in middle Pleistocene Europe. Quat Sci Rev 30:1511–1524

Falguères C, Shao Q, Han F, Bahain JJ, Richard M, Perrenoud C, Moigne AM, Lumley de H (2015) New ESR and U-series dating at Caune de l'Arago, France: a key-site for European middle Pleistocene. Quat Geochronol 30:547–553

Gómez-Robles A, Martinón-Torres M, Bermúdez de Castro JM, Margvelashvili A, Bastir M, Arsuaga JL, Pérez-Pérez A, Estebaranz F, Martínez LM (2007) A geometric morphometric analysis of hominin upper first molar shape. J Hum Evol 53:272–285

Gómez-Robles A, Martinón-Torres M, Bermúdez de Castro JM, Prado-Simón L, Arsuaga JL (2011) A geometric morphometric analysis of hominin upper premolars. Shape variation and morphological integration. J Hum Evol 61:688–702

Grine FE (2002) Scaling of tooth enamel thickness, and molar crown size reduction in modern humans. S Afr J Sci 9:503–509

Grine FE (2005) Enamel thickness of deciduous and permanent molars in modern Homo sapiens. Am J Phys Anthropol 126:14–31

Guipert G, de Lumley M-A, Tuffreau A, Mafart B (2011) A late middle Pleistocene hominid: Biache-saint-Vaast 2, North France. CR Palevol 10:21–33

Hanegraef H, Martinón-Torres M, Martínez de Pinillos M, Martín-Francés L, Vialet A, Arsuaga JL, Bermúdez de Castro JM (2018) Dentine morphology of Atapuerca-Sima de los Huesos lower molars: evolutionary implications through three-dimensional geometric morphometric analysis. Am J Phys Anthropol 166:276–295

Hershkovitz I, May H, Sarig R, Pokhojaev A, Grimaud-Hervé D, Bruner E, Fornai C, Quam R, Arsuaga JL, Krenn VA, Martinón-Torres M, de Castro JMB, Martín-Francés L, Slon V, Albessard-Ball L, Vialet A, Schüler T, Manzi G, Profico A et al (2021) A middle Pleistocene *homo* from Nesher Ramla, Israel. Science 372:1424–1428

Horvath JE, Ramachandran GL, Fedrigo O, Nielsen WJ, Babbitt CC (2014) Genetic comparisons yield insight into the evolution of enamel thickness during human evolution. J Hum Evol 73:75–87

Hublin J-J, Roebroeks W (2009) Ebb and flow or regional extinctions? On the character of Neandertal occupation of northern environments. CR Palevol 8:503–509

Hublin JJ (2009) The origin of Neandertals. PNAS 106:16022–16027

Huxtable J, Aikten MJ (1988) Datation par thermoluminescence. In: Tuffreau A, Sommé J (eds) Le gisement paléolithique moyen de Biache-Saint-Vaast (Pas-de-Calais). Stratigraphie, environnement études archéologiques, (1re partie). edn. Mémoires de la Société Préhistorique Française, Paris, pp 107–108

Kono RT (2004) Molar enamel thickness and distribution patterns in extant great apes and humans: new insights based on a 3-dimensional whole crown perspective. Anthropol Sci 112:121–146

Kupczik K, Hublin J-J (2010) Mandibular molar root morphology in Neanderthals and Late Pleistocene and recent Homo sapiens. J Hum Evol 59:525–541

Lieberman DE (2011) The evolution of the human head. Harvard University Press, Cambridge

Lisiecki LE, Raymo ME (2005) A Pliocene-Pleistocene stack of 57 globally distributed benthic δ18O records. Paleoceanography 20

Lucas P, Constantino P, Wood B, Lawn B (2008) Dental enamel as a dietary indicator in mammals. BioEssays 30:374–385

Macchiarelli R, Bayle P, Bondioli L, Mazurier A, Zanolli C (2013) From outer to inner structural morphology in dental anthropology: integration of the third dimension in the visualization and quantitative analysis of fossil remains. In: Scott GR, Irish JD (eds) Anthropological perspectives on tooth morphology. Genetics, evolution, variation. Cambridge University Press, Cambridge, pp 250–277

Macchiarelli R, Bondioli L, Debenath A, Mazurier A, Tournepiche J-F, Birch W, Dean MC (2006) How Neanderthal molar teeth grew. Nature 444:748–751

MacDonald K, Martinón-Torres M, Dennell RW, Bermúdez de Castro JM (2012) Discontinuity in the record for hominin occupation in South-Western Europe: implications for occupation of the middle latitudes of Europe. Quat Int 271:84–97

Manzi G (2016) Humans of the middle Pleistocene: the controversial calvarium from Ceprano (Italy) and its significance for the origin and variability of Homo heidelbergensis. Quat Int 411:254–261

Martín-Francés L, Martinón-Torres M, Martínez de Pinillos M, García-Campos C, Modesto-Mata M, Zanolli C, Rodríguez L, Bermúdez de Castro JM (2018) Tooth crown tissue proportions and enamel thickness in Early Pleistocene *Homo antecessor* molars (Atapuerca, Spain). PLoS One 13:e0203334

Martín-Francés L, Martinón-Torres M, Martínez de Pinillos M, García-Campos C, Zanolli C, Bayle P, Modesto-Mata M, Arsuaga JL, Bermúdez de Castro JM (2020) Crown tissue proportions and enamel thickness distribution in the middle Pleistocene hominin molars from Sima de los Huesos (SH) population (Atapuerca, Spain). PLoS One 15:e0233281

Martínez de Pinillos M, Martín-Francés L, de Castro JMB, García-Campos C, Modesto-Mata M, Martinón-Torres M, Vialet A (2020) Inner morphological and metric characterization of the molar remains from the Montmaurin-La niche mandible: the Neanderthal signal. J Hum Evol 145:102739

Martínez de Pinillos M, Martinón-Torres M, Martín-Francés L, Arsuaga JL, Bermúdez de Castro JM (2017) Comparative analysis of the trigonid crests patterns in *Homo antecessor* molars at the enamel and dentine surfaces. Quat Int 433:189–198

Martinón-Torres M, Bermúdez de Castro JM, Gómez-Robles A, Prado-Simón L, Arsuaga JL (2012) Morphological description and comparison of the dental remains from Atapuerca-Sima de los Huesos site (Spain). J Hum Evol 62:7–58

Martinón-Torres M, Bermúdez de Castro JM, Martínez de Pinillos M, Modesto-Mata M, Xing S, Martín-Francés L, García-Campos C, Wu X, Liu W (2019) New permanent teeth from gran Dolina-TD6 (sierra de Atapuerca). The bearing of Homo antecessor on the evolutionary scenario of early and middle Pleistocene Europe. J Hum Evol 127:93–117

Martinón-Torres M, Spěváčková P, Gracia-Téllez A, Martínez I, Bruner E, Arsuaga JL, Bermúdez de Castro JM (2013) Morphometric analysis of molars in a middle Pleistocene population shows a mosaic of 'modern' and Neanderthal features. J Anat 223:353–363

Maureille B, Rougier H, Houet F, Vandermeersch B (2001) Les dents inférieures du Néandertalien Regourdou 1 (site de Regourdou, commune de Montignac, Dordogne): analyses métriques et comparatives. Paleo 13:183–200

Mitteroecker P, Bookstein F (2011) Linear discrimination, ordination, and the visualization of selection gradients in modern morphometrics. Evol Biol 38:100–114

Mitteroecker P, Gunz P, Windhager S, Schaefer K (2013) A brief review of shape, form, and allometry in geometric morphometrics, with applications to human facial morphology. Hystrix 24:59–66

Molnar S (1971) Human tooth wear, tooth function and cultural variability. Am J Phys Anthropol 34:175–189

Olejniczak AJ, Smith TM, Feeney RNM, Macchiarelli R, Mazurier A, Bondioli L, Rosas A, Fortea J, de la Rasilla M, Garcia-Tabernero A, Radovcic J, Skinner MM, Toussaint M, Hublin J-J (2008) Dental tissue proportions and enamel thickness in Neandertal and modern human molars. J Hum Evol 55:12–23

Ortiz A, Skinner MM, Bailey SE, Hublin J-J (2012) Carabelli's trait revisited: an examination of mesiolingual features at the enamel–dentine junction and enamel surface of pan and Homo sapiens upper molars. J Hum Evol 63:586–596

Roksandic M (2016) The role of the Central Balkans in the peopling of Europe: paleoanthropological evidence. In: Harvati K, Roksandic M (eds) Paleoanthropology of the Balkans and Anatolia: human evolution and its context. Springer, Netherlands, Dordrecht, pp 15–33

Roksandic M, Mihailović D, Mercier N, Dimitrijević V, Morley MW, Rakočević Z, Mihailović B, Guibert P, Babb J (2011) A human mandible (BH-1) from the Pleistocene deposits of Mala Balanica cave (Sićevo gorge, Niš, Serbia). J Hum Evol 61:186–196

Rosas A (2001) Occurrence of Neanderthal features in mandibles from the Atapuerca SH-site. Am J Phys Anthropol 114:74–91

Rougier H (2003) Étude descriptive et comparative de Biache-saint-Vaast 1, Biache-saint-Vaast, Pais de Calais, (France). Sciences de l´Homme et Société. Université de Bordeaux I, PhD, p 418

Scolan H, Santos F, Tillier AM, Maureille B, Quintard A (2012) Des nouveaux vestiges néanderthaliens à las Pélénos (Monsempron-Libos, lot-et-Garonne, France). Bull Mém Soc Anthropol Paris 24:69–95

Skinner MM, de Vries D, Gunz P, Kupczik K, Klassen RP, Hublin J-J, Roksandic M (2016) A dental perspective on the taxonomic affinity of the Balanica mandible (BH-1). J Hum Evol 93:63–81

Smith TM, Olejniczak AJ, Zermeno JP, Tafforeau P, Skinner MM, Hoffmann A, Radovçiá J, Toussaint M, Kruszynski R, Menter C, Moggi-Cecchi J, Glasmacher UA, Kullmer O, Schrenk F, Stringer C, Hublin J-J (2012) Variation in enamel thickness within the genus homo. J Hum Evol 62:395–411

Smith TM, Toussaint M, Reid DJ, Olejniczak AJ, Hublin J-J (2007) Rapid dental development in a middle Paleolithic Belgian Neanderthal. PNAS 10:20220–20225

Sommé J (1988) Chronostratigraphie et environnement. In: Tuffreau, A., Sommé, J. (Eds.), Le gisement paléolithique moyen de Biache-Saint-Vaast (Pas-de-Calais). Stratigraphie, environnement études archéologiques (1re partie). Mémoires de la Société Préhistorique Française, Paris, pp 27–45

Trinkhaus E (1990) Cladistics and the hominid fossil record. Am J Phys Anthropol 83:1–11

Tuffreau A (1978) Les fouilles du gisement paléolitique de Biache-saint-Vaast (Pas-de-Calais): annés 1976 et a1977-premiers résultats. Bulletin de la Association française pour l´étude du. Quaternaire 15:46–55

Tuffreau A (1988) Historique des fouilles à Biache-saint-Vaast, in: Tuffreau A, Sommé J (Eds.). Le gisement paléolithique moyen de Biache-saint-Vaast (Pas-de-Calais). Stratigraphie, environnement études archéologiques (1re partie). Mémoires de la Société Préhistorique Française, Paris, pp 15–24

Tuffreau A, Munaut AV, Puisseégur JJ, Sommé J (1982) Stratigraphie et environment de la sequence archéologique de Biache-saint Vaast (Pas-de-Calais). Bulletin de la Association française pour l´étude du. Quaternaire 19:57–61

Turner CG II, Nichol CR, Scott GR (1991) Scoring procedures for key morphological traits of the permanent dentition: the Arizona State University dental anthropology system. In: Kelley M, Larsen C (eds) Advances in dental anthropology. Wiley-Liss, New York, pp 13–31

Vandermeersch B (1978) Étude préliminaire du crâne humain du gisement paléolithique de Biache-saint-Vaast (Pas-de-Calais). Bulletin de la Association française pour l´étude du. Quaternaire 54-55-56:65–67

Vandermeersch B (1982) L'Homme de Biache-saint-Vaast. Comparaison avec l'Homme de Tautavel. In: CNRS (ed) 1er Congrès international de Paléontologie Humaine. L'Homo erectus et la place de l'Homme de Tautavel parmi les Hominidés Fossiles, Nice, pp 894–900

Vialet A, Modesto-Mata M, Martinón-Torres M, Martínez de Pinillos M, Bermúdez de Castro J-M (2018) A reassessment of the Montmaurin-La niche mandible (haute Garonne, France) in the context of European Pleistocene human evolution. PLoS One 13:e0189714

Wolpoff MH (1979) The Krapina dental remains. Am J Phys Anthropol 50:67–114

Yokoyama Y (1989) Direct gamma-ray spectrometric dating of Anteneandertalian and Neandertalian remains. In: Giacobini G (ed) Hominidae, proceedings of the 2nd intern. Congress of Human Paleontology, Turin, pp 387–390

Yokoyama Y, Falgueres C, Quaegebeur JP (1985) ESR dating of quartz from quaternary sediments: first attempt. Nucl Tracks Rad Measure 1982(10):921–928

Yokoyama Y, Nguyen HV (1981) Datation directe de I'Homme de Tautavel par la spectrométrie gamma, non destructive, du crane humanin fossile Arago XXI. C R Sci Paris 292:741–744

Zanolli C, Biglari F, Mashkour M, Abdi K, Monchot H, Debue K, Mazurier A, Bayle P, Le Luyer M, Rougier H, Trinkaus E, Macchiarelli R (2019) A Neanderthal from the Central Western Zagros, Iran. Structural reassessment of the Wezmeh 1 maxillary premolar. J Hum Evol 135:102643

Zanolli C, Martinón-Torres M, Bernardini F, Boschian G, Coppa A, Dreossi D, Mancini L, Martínez de Pinillos M, Martín-Francés L, Bermúdez de Castro JM, Tozzi C, Tuniz C, Macchiarelli R (2018) The middle Pleistocene (MIS 12) human dental remains from Fontana Ranuccio (Latium) and Visogliano (Friuli-Venezia Giulia), Italy. A comparative high resolution endostructural assessment. PLoS One 13:e0189773